Electrical Engineering Department
California Polytechnic State University

Senior Project Report

Audio Loop Station

Samuel Montoya Lopez

Professor Taufik

Abstract

A digital loop station is an electronic device that takes an analog audio signal, samples it with an Analog-to-Digital converter, stores it digitally in a system memory, and repeatedly outputs the content to a Digital-to-Analog converter. The signal is controlled by use of a microcontroller and amplified by external circuitry. The purpose of a digital loop station is to record and store an audio sample in real-time then playback the stored signal and superimpose additional audio signals over it. This project details a 16-bit digital loop station that samples at a rate of 44.1 kHz which is the industry standard for CD quality music. This loop station has three functions available to the user – record, playback, or reset. Tests performed on the prototype demonstrated successful operation of the digital loop station. Two issues remain unresolved: high frequency noise at the analog output and a slight discontinuity in the processed audio waveform.

Acknowledgements

This paper culminates the pursuit of an undergraduate degree that has spanned over a hundred courses at two colleges, four internships across the state, and the greater part of my mental bandwidth over these past few years. I would like to express my deepest gratitude to a few people who have been instrumental in my success.

To my good friend Oscar Daza as well as my lifelong friend Luis Dominguez for lighting a fire in me and giving me the impetus to go back to school at the age of twenty-six. These Cal Poly alumni convinced me that if they can complete an engineering program, then I could too.

To Sammy Solis, my closest friend and accomplice, who was with me at the start of this journey and has pushed me more than anyone else, and Tomas Pirir, my very first lab partner, most trusted confidante, and *Dream Team* alum for making it all the way to the end with me.

Professor Taufik for being a most helpful teacher, for his ceaseless patience, and for being stern with me when I needed it. To my friend Jeff Pankau for helping me fill in the missing pieces for this project. To my best mate at Cal Poly, Willy Raga Okpobua, for the hundreds of late nights and thousands of hours that we studied together. To my dear friend and mentor Grace RaeLyn Larson for her unending emotional and moral support.

To my father, Manuel Lopez Chavez, who is the single most influential person in my life, and my mother Maria del Rocio Lopez Montoya for her endless encouragement. My siblings Manuel and Rocio for being with me every step of the way.

To my beautiful and loving daughter Mary Luz Lopez for inspiring me to take on such a long and strenuous journey, for keeping me strong all these years, and for giving me the resolve to see it through. Mostly, for making me a better father and a better man.

Table of Contents

List of Figures

List of Tables

Chapter 1

Introduction

The idea behind live looping is for individual musicians to present themselves as multiple performers. The musician first plays a sample of music into a device known as a 'loop station' or 'loop pedal' which records the audio signal in real-time. Once recorded, the sample of music repeats or 'loops' indefinitely. Musicians utilize foot-controlled switches to place the loop pedal in 'play','record', or 'reset' mode which allows the user to scrub the recorded sample. Additionally, there exists a bypass path from input to output to stack multiple audio signals.

1.1 History

Looping is a musical phenomenon pioneered by legendary electric guitarist and inventor Les Paul whose signature guitar bears his name. Paul recorded samples of music using a tape-reel and then played over himself during live show performances. This was an impressive feat for the pre-digital era; however, it required an exhaustive setup with multiple reels and the concept of looping remained a fringe practice in the musical community [1]. Les Paul and others experimented with multitrack recording throughout the second half of the twentieth century but were limited to studio recording [2].

Figure 1.1: Various Audio Pedals

In the dawn of the American music industry, guitar effects were produced manually; reverb was accomplished by placing an amplifier in a chamber or by playing in a large hall, delay or echo was created by using multiple tape recorders slightly out of sync, chorus was accomplished by rotating a speaker with a motor, etc [3]. In 1956 Walter B. Shockley, John Bardeen, and Walter H. Brattain won the Nobel Prize in Physics for their invention of the transistor at Bell Laboratories, and

inadvertently changed the music industry forever [4]. During the rock era of the 1960's, guitarists began using processed audio signals such as distortion – an effect produced by a clipping circuit. Pedal operated devices, such as those shown in Figure 1.1, gained popularity amongst American and English bands and became the norm in all genres of music from rock and funk to country and jazz [5]. Pedal operated devices or 'guitar pedals' were preferred for their portability as opposed to studio effects. Initially, all guitar pedals consisted of analog circuitry and used a mix of operational amplifiers, tubes, transistors, resistors, and capacitors [6]. Digitized audio began occurring in the 1970's as microcontrollers became faster and more cost-effective. Once converted to binary, a digital audio signal can reproduce analog effects such as delay, phase shifting, overdrive, and chorus [7]. Additionally, digital audio allows the innovation of new effects not possible with analog circuitry.

Figure 1.2: Echoplex Digital Pro [8]

The loop station or 'loop pedal' combined live looping into a guitar pedal, making it a possibility for the performing musician [9]. The first mass produced loop pedals appeared in the early 1990's such as the Lexicon JamMan and the Echoplex Digital Pro, shown in Figure 1.2. Initially, a loop station could only perform one task: loop a single audio sample. Over time transistors size decreased, memory became cheaper, and digital hardware was easier to manufacture, leading to multi-layer tracking on a single loop pedal. Today, numerous companies such as Boss, Electro-Harmonics, and TC Electronics produce loop stations varying in complexity and cost. Once a hobby for fringe guitarists, live looping is now commonplace amongst musicians and every working musician owns or has owned a loop station [10].

Chapter 2

Background

There is wide demand for audio looping in the music industry and numerous approaches exist to develop looping methods.

2.1 Extracting Audio Loops

In the paper "Music Loop Extraction from Digital Audio Signals," pattern-recognition techniques identify and extract audio samples in existing tracks that are ideal for looping [11]. In "Drum Loop Pattern Extraction from Polyphonic Music," a pattern method characterizes the prominent repeating structure of the beats [12]. While both papers are useful in creating loops from recorded music, the approach is purely digital whereas the project in this paper requires an input and output analog signal. Additionally, these methods rely on creating audio loops from recorded music already in the digital domain, whereas a loop station creates a loop from an audio signal in real-time.

2.2 Audible Frequency Range

The frequency of a signal determines its pitch, and the human audible frequency spectrum lies between 20 Hz and 20 kHz [13]. Frequencies beyond this range are undesirable and require filtering. Digital filtering is a modern approach detailed in the paper "Digital Filters for High Performance Audio Delta-Sigma Analog-to-Digital and Digital-to-Analog Conversions". Using this approach, a multi-stage comb filter combines with a single-stage FIR (Finite Impulse Response) filter [14]. An analog approach uses easily designed Sallen-Key filters to fine-tune sharp cutoff regions, quality factor, and center frequencies. Additionally, cascading lowpass and highpass filters in stages allows for easily derived transfer functions described in the landmark 1952 paper "A Practical Method of Designing RC Active Filters" by R. P. Sallen and E. L. Key [15].

2.3 Power Considerations

Audio waveforms are sinusoidal and require a bipolar DC power source. Audio pedals, valued for their portability, are usually powered by batteries. There are multiple ways to create a bipolar power supply from single-supply batteries. One approach is to reference ground at the output of a buck or boost converter to produce a negative voltage from a positive DC source as shown in Figure 2.1.

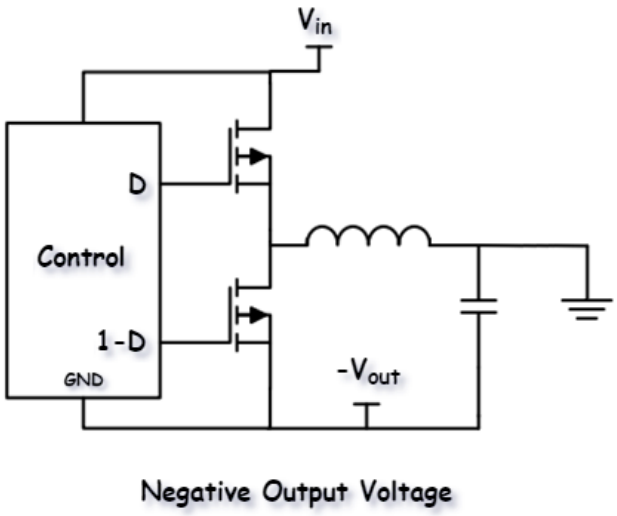

Figure 2.1: Buck Converter Producing Negative Voltage [16]

The positive source and negative output then provide bipolar power to a circuit. Alternatively, center-tapping a ground node between an even number of batteries is possible. This project uses a less expensive approach; a resistor divider creates an offset voltage midway between supply voltage and ground. The audio waveform references the offset voltage for the ADC (Analog-to-Digital Converter) and DAC (Digital-to-Analog Converter) stages. This approach reduces complexity and cost at the expense of efficiency.

2.4 Objective

The goal of this project is to design a loop station that sends an audio signal both through a bypass path to the output stage and to an digital processing stage by use of a microcontroller. Users control the state of the loop pedal – 'play', 'record', or 'reset' – with footswitches. Loop pedals typically feature a single switch which puts a steep learning curve on the user. This is because users activate multiple states with various switch-controlled actions - single tap, tap and hold, double tap, etc. The loop pedal built in this project reduces complexity by featuring two switches each controlled by a single tap. LEDs (Light Emitting Diodes) provide visual feedback which indicate the state of the pedal to the user. The loop pedal built in this project features one recorded digital track and a parallel bypassed analog signal.

Chapter 3

Design Requirements

Loop stations by different makers will have varying features and options. The most common feature is the ability to record multiple tracks atop each other in the memory. Other options include tempo correction, non-volatile memory storage, built-in metronome, and audio effects [17].

3.1 Minimum Requirements

A loop station requires the following minimum components: ADC, DAC, memory storage, microcontroller or FPGA, buffers, switches, transistors, and passive components. Programming the device requires a fundamental understanding of firmware and communication protocols. Industry standards typically adhere to the following specifications and limits: loop pedals sample either 16 or 24 bits at 44.1 kHz, switch delays must be less than 30 ms, distortion and noise, both undesirable traits, are noticeable in the millivolt range and corrupt the signal, and the integrity of the original signal must remain wholly intact in both the sampled path and the parallel undisturbed path [18, 19].

3.2 Loop Pedal Description

The following is a short explanation on the mechanics of a modern loop pedal. An instrumentalist or musician presses a footswitch on a loop station which begins the recording process. Simultaneously, the musician plays a short audio sample or 'vamp' into the pedal. The audio is converted and recorded digitally as the user is playing until a second tap on the footswitch is pressed. The microprocessor then ceases recording and plays back the stored audio sample from beginning to end. The audio sample is repeated continuously until another tap on the footswitch occurs. Concurrently, a parallel path allows the unaffected input signal to sum with the processed signal at the output. This is commonly referred to as 'true bypass'.

3.3 System Diagrams

The Level Zero system diagram, shown in Figure 3.1, demonstrates the inputs and outputs of the loop station at a system level. The user provides power in the form of three AA batteries (3 x 1.5 V_{DC}) that control the power flow with a switch. Two switches determine the state of the processor and a potentiometer controls the volume. The unit has an analog audio output as well as three LEDs which provide feedback signifying what state the unit is in.

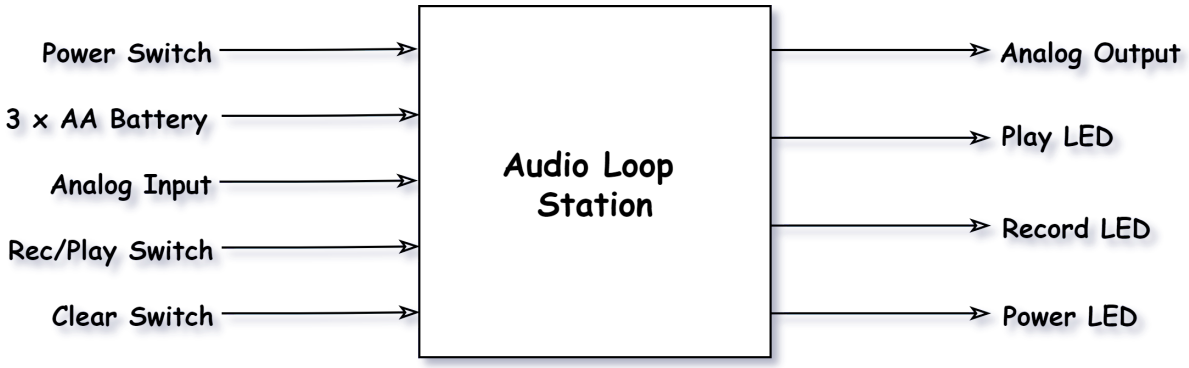

Figure 3.1: Level Zero System Diagram

The Level One system diagram as shown in Figure 3.2 demonstrates the embedded system of the circuit. When the user closes the switch the system powers on. An LDO (Low-Dropout Regulator) then powers the ADC, SRAM (Static Random-Access Memory), DAC, microcontroller, and various op-amps and transistors. After being filtered, the input audio signal is sent to the 16-bit ADC and sampled by the microcontroller at 44.1 kHz. When the system is in the record state, the microcontroller stores the data from the ADC in the SRAM. The input analog signal simultaneously connects to a summing circuit at the final stage. Pressing the Rec/Play switch places the system in the recording state. When the system is in the 'play' state, the microcontroller empties the contents of the SRAM to the DAC. This allows the processed signal and the input signal to sum together. The system holds three LEDs controlled by the microcontroller which indicate power-on and the two states of the system. An external potentiometer in the DAC circuit controls the volume of the processed signal.

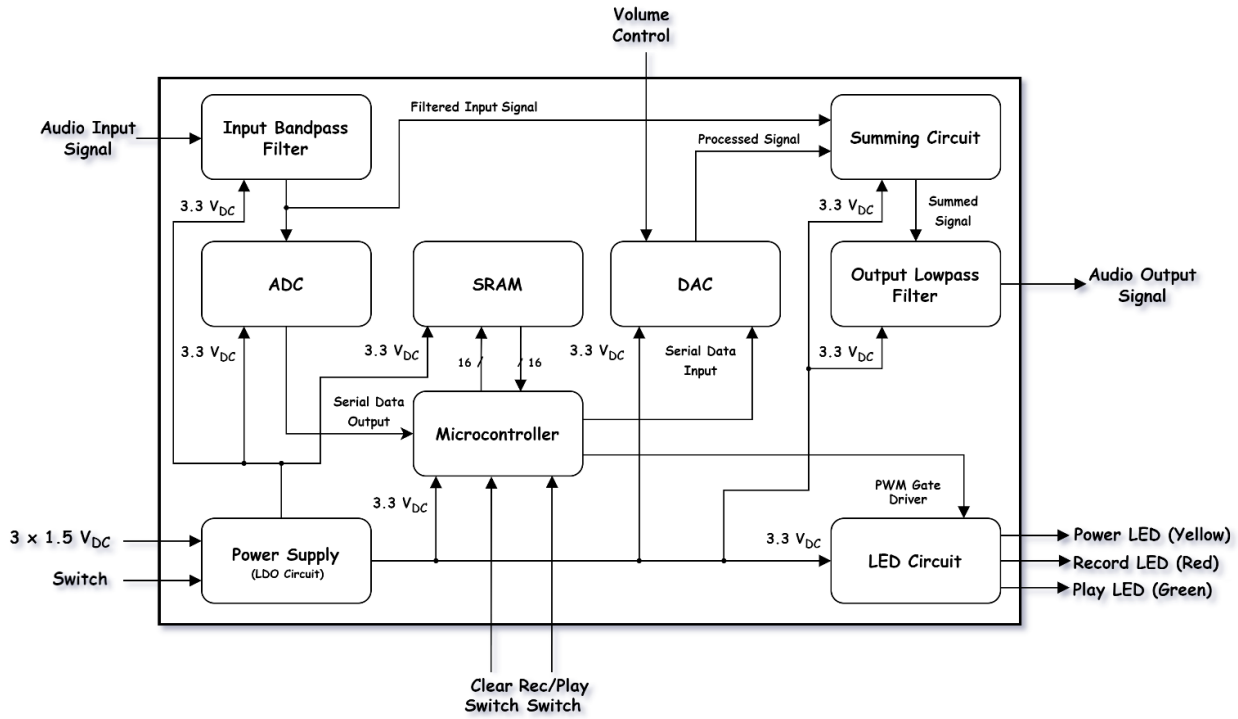

Figure 3.2: Level One Block Diagram

3.4 Functional Requirements

Table 3.1 displays the functional requirements for the power supply circuit built from the LDO LP5907 chip [20].

Table 3.1: Power Supply Functional Requirements

Module	Power Supply
Input	• 3 x 1.5 V_{DC} AA batteries • Single-Pole-Single-Throw Switch
Output	• 3.3 V_{DC} at 250 mA_{max}
Functionality	Supplies Power to Modules

Table 3.2 displays the functional requirements for the input bandpass filter circuit from the op-amp OPA2376 [21].

Table 3.2: Input Bandpass Filter Functional Requirements

Module	Input Bandpass Filter
Input	• Audio Input Signal • 3.3 V_{DC} from Power Supply at 760 μA_{max}
Output	• Filtered Input Signal
Functionality	Eliminates Frequencies Outside Audible Range

Table 3.3 displays the functional requirements for the ADC circuit built from the LTC1864 chip [22].

Table 3.3: ADC Functional Requirements

Module	Analog-to-Digital Converter
Input	• Filtered Input Signal • 3.3 V_{DC} from Power Supply at 8.5 mA_{max} • Serial Clock from Microcontroller • Chip Select from Microcontroller
Output	• Serial Data Output to Microcontroller
Functionality	Transforms Filtered Signal to Digital Information

Table 3.4 displays the functional requirements for the DAC circuit built from the DAC8830 chip [23]. The DNL (Differential Non-Linearity) is $DNL_k < 1$ and the INL (Integrated Non-Linearity) is $INL_k < 2$ which is compliant with audio standards.

Table 3.4: DAC Functional Requirements

Module	Digital-to-Analog Converter
Input	• Serial Data Input • 3.3 V_{DC} from Power Supply at 20 μA_{max} • Serial Clock from Microcontroller • Chip Select from Microcontroller
Output	• Processed Audio Signal
Functionality	Transforms Digital Information to Analog Output

Table 3.5 displays the functional requirements for the summing circuit built from the op-amp OPA2376 [21].

Table 3.5: Summing Circuit Functional Requirements

Module	Summing Circuit
Input	• 3.3 V_{DC} from Power Supply at 760 μA_{max} • Filtered Input Signal • Processed Signal
Output	• Summed Audio Signal
Functionality	Sums Audio Input Signal and Processed Signal

Table 3.6 displays the functional requirements for the input bandpass filter circuit from the op-amp OPA2376 [21].

Table 3.6: Output Lowpass Filter Functional Requirements

Module	Output Lowpass Filter
Input	• Summed Audio Signal • 3.3 V_{DC} from Power Supply at 760 μA_{max}
Output	• Filtered Output Signal
Functionality	Eliminates Noise

Table 3.7 displays the functional requirements for the microcontroller which is the Renesas R7FS5D57C3A01CFB#AA0 [24].

Table 3.7: Microcontroller Functional Requirements

Module	Microcontroller
Input	• 3.3 V_{DC} from Power Supply at 102 mA_{max}
	• Clear Switch Signal
	• Rec/Play Signal
	• Serial ADC Data
	• DAC Bits D_0-D_{15}
Output	• ADC Bits A_0-A_{20}
	• Serial Clock
	• Serial DAC Data
	• LED Signals
	• Chip Select to ADC
	• Chip Select to DAC
	• Read Signal to System Memory
	• Write Signal to System Memory
	• Chip Select to System Memory
Functionality	Controls Data Flow, User Feedback, and State of System

Table 3.8 displays the functional requirements for the system memory circuit built upon the SRAM CY62167DV30LL chip [25]. There are 2^{20} = 1,048,576 address spaces on the system memory which gives enough memory for at least twenty seconds of audio as seen in Equation 3.1.

$$Time = \ 1,048,576 \ address \ spaces \ * \ \frac{1 \ second}{44,100 \ address \ spaces} \approx 23 \ seconds \tag{3.1}$$

Table 3.8: System Memory Functional Requirements

Module	System Memory
Input	• 3.3 V_{DC} from Power Supply at 25 mA_{max}
	• Read Signal from Microcontroller
	• Write Signal from Microcontroller
	• Chip Select from Microcontroller
	• ADC Bits A_0-A_{19}
Output	• DAC Bits D_0-D_{15}
Functionality	Stores Data from ADC and Outputs to DAC

Table 3.9 displays the functional requirements for the LED Circuit. This circuit provides user feedback.

Table 3.9: LED Circuit Functional Requirements

Module	LED Circuit
Input	• 3.3 V_{DC} from Power Supply at 60 mA_{max}
	• PWM signals GPIO Pins from Microcontroller
Output	• 3 × LED
Functionality	User Feedback Indicating Power/State

Chapter 4

Design and Simulation

Each module of the system has a unique set of challenges to overcome, such as powering every stage from a single source, fine-tuning the frequency response, and preserving the audio signal from analog to digital and back to analog. Equations and simulations confirm the behavior of the system before the design is implemented in hardware.

4.1 Power Supply Circuit

Three AA batteries (3×1.5 V_{DC}) in series supply 4.5 V_{DC} at the power source as shown in Figure 4.1. This configuration powers an LDO that steps down the voltage to 3.3 V_{DC} and powers every module in the system. The LDO circuit consists of an input capacitor, several output capacitors, and a Texas Instruments LP5907 chip. The ENA (Enable) pin on the LDO is permanently tied to the V_{in} pin giving the user full control of power flow by use of an SPST (Single-Pole-Single-Throw) switch.

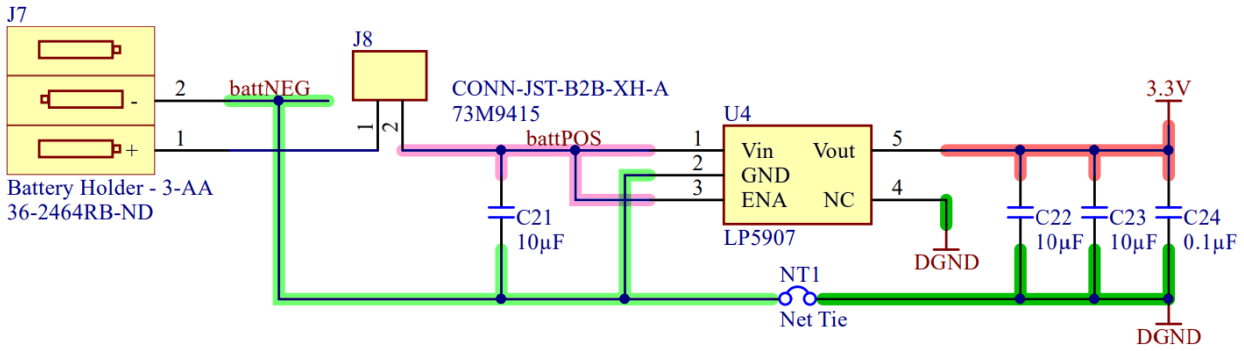

Figure 4.1: Power Supply Circuit

A resistor divider splits the 3.3 V_{DC} from the LDO to $V_{offset} = 3.3$ $V_{DC}/2$ as shown in Figure 4.2. The resistor values of R_{14} and R_{16} are sized large enough to minimize power consumption across the divider but not so large to introduce significant thermal noise. The two capacitors in parallel with R_{16} filter noise and prevent oscillations at V_{offset}. This offset voltage centers the audio waveform at the ADC and DAC converter circuits.

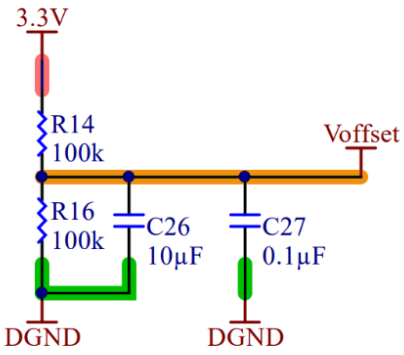

Figure 4.2: Resistor Divider Splits 3.3 V_{DC} into V_{offset}

4.2 Input Bandpass Filter

The pre-ADC circuit is a two-stage bandpass filter – a passive lowpass filter and a passive highpass filter – as shown in Figure 4.3. The lowpass filter references digital ground and the highpass filter references V_{offset} to center the audio signal midway between 3.3 V_{DC} and ground. The output of the bandpass filter connects to a voltage-follower which prevents loading from the rest of the system.

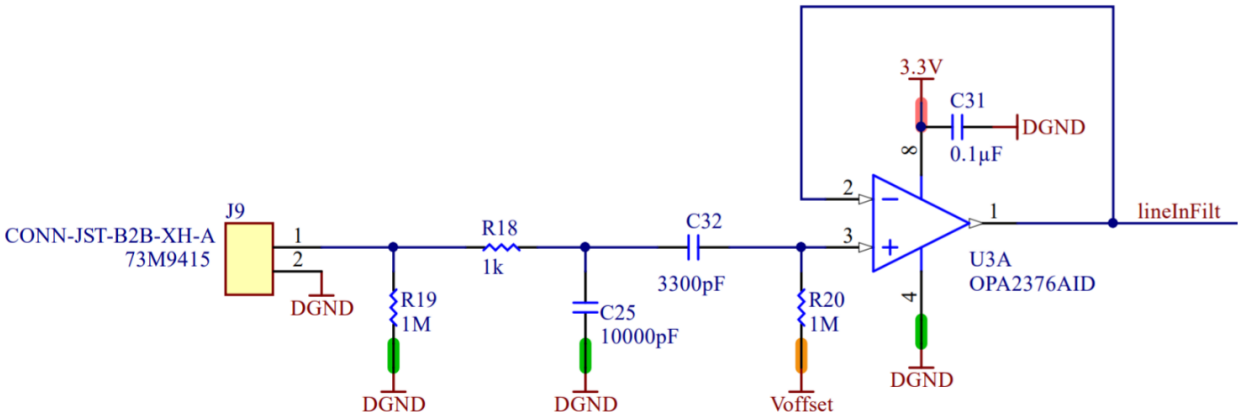

Figure 4.3: Input Bandpass Filter

Equation 4.1 shows the full transfer function of the bandpass filter and Equation 4.2 organizes the transfer function into a format that facilitates a derivation of the key variables.

$$H(s) = \frac{sC_{32}R_{20}}{s^2C_{32}C_{25}R_{18}R_{20} + s(C_{32}R_{20} + C_{25}R_{18} + R_{18}C_{32}) + 1} \tag{4.1}$$

$$H(s) = \frac{k\,\frac{\omega_o}{Q}s}{s^2 + \frac{\omega_o}{Q}s + \omega_o^2} = \frac{\frac{1}{C_{25}R_{18}}s}{s^2 + \left(\frac{1}{C_{25}R_{18}} + \frac{1}{C_{32}R_{20}} + \frac{1}{C_{25}R_{20}}\right)s + \frac{1}{C_{32}C_{25}R_{18}R_{20}}} \tag{4.2}$$

Equations 4.3 and 4.4 define the center frequency f_o and bandwidth Δf from the variables in the transfer function. Equation 4.5 demonstrates the quality factor Q of the bandpass filter.

$$f_o = \frac{\omega_o}{2\pi} = \frac{1}{2\pi}\sqrt{\frac{1}{C_{32}C_{25}R_{18}R_{20}}} = 876\ Hz \tag{4.3}$$

$$\Delta f = \frac{1}{2\pi} * \frac{\omega_o}{Q} = \frac{1}{2\pi}\left(\frac{1}{C_{25}R_{18}} + \frac{1}{C_{32}R_{20}} + \frac{1}{C_{25}R_{20}}\right) = 15.98\ kHz \tag{4.4}$$

$$Q = \frac{f_o}{\Delta f} = 0.054827 \tag{4.5}$$

Equation 4.6 and Equation 4.7 demonstrate the derivation of the corner frequencies of the bandpass filter from the center frequency and the quality factor. A simulated bode plot of the bandpass filter, shown in Figure 4.4, confirms the variables in Equations 4.3 – 4.7.

$$f_{c-lo} = f_0\left(\sqrt{1 + \frac{1}{4Q^2}} - \frac{1}{2Q}\right) = 48\ Hz \tag{4.6}$$

$$f_{c-hi} = f_0\left(\sqrt{1 + \frac{1}{4Q^2}} + \frac{1}{2Q}\right) = \ 16.03\ kHz \tag{4.7}$$

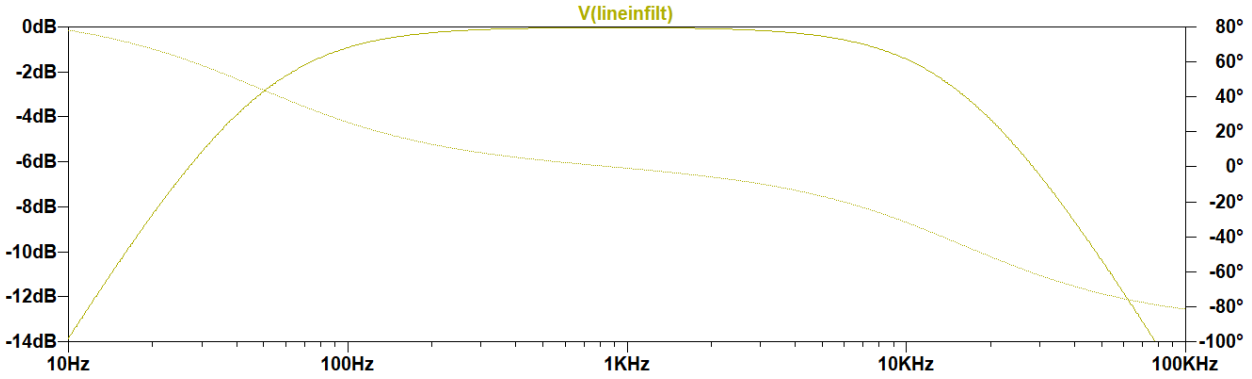

Figure 4.4: Bode Plot Simulation of the Input Bandpass Filter

Equation 4.8 shows the phase ϕ of the bandpass filter calculated in degrees.

$$\phi = \angle H(\omega) = \frac{180\ ^\circ}{\pi} * tan^{-1}\left(\frac{Q(\omega_o^2 - \omega^2)}{\omega_o\omega}\right) \tag{4.8}$$

Figure 4.5 shows the simulated results of the input bandpass filter in the time domain. Note that the audio input signal references digital ground whereas the signal at the node lineInFilt references $V_{offset} = 3.3\ V_{DC}/2$.

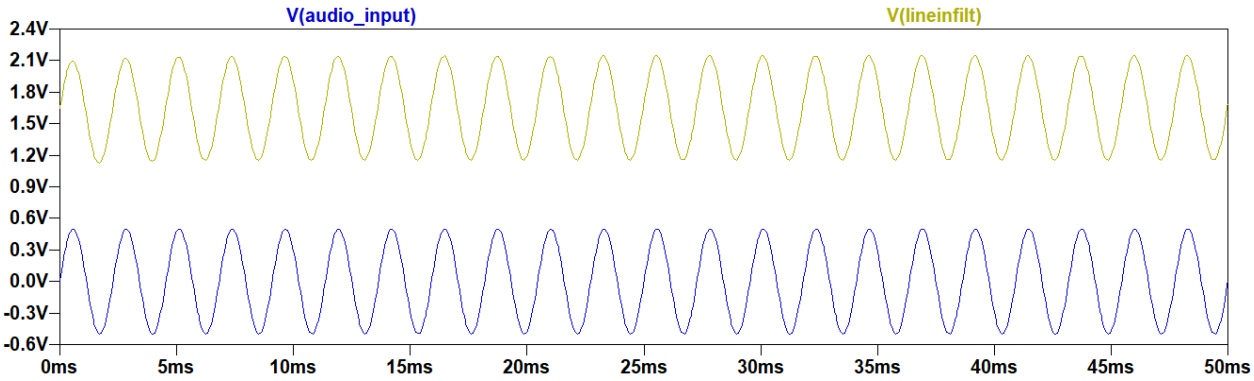

Figure 4.5: Simulation of Audio Input and lineInFilt

4.3 Analog-to-Digital Converter

The node lineInFilt connects to both the 16-bit LTC1864 SAR (Successive-Approximation-Register) Analog-to-Digital converter, shown in Figure 4.6, and the summing amplifier. A passive 1st order lowpass filter blocks high frequencies from the clock which would otherwise compromise the integrity of the audio signal. The serial data is the output of the ADC.

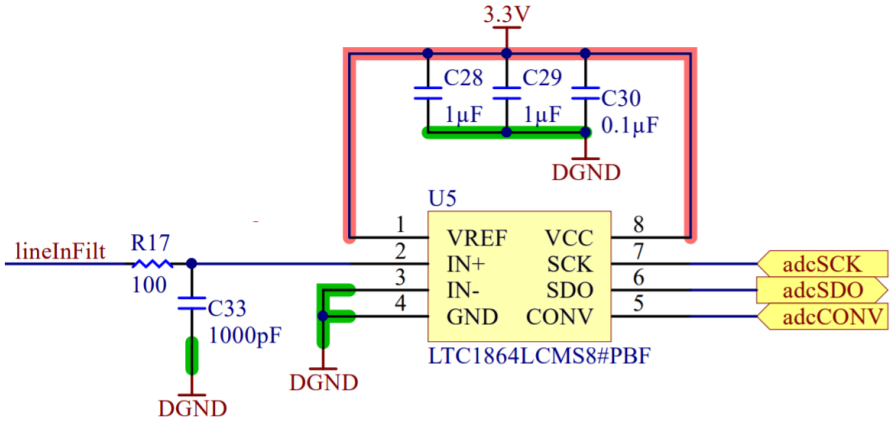

Figure 4.6: Analog-to-Digital Converter Circuit

Equations 4.9 shows the transfer function and Equation 4.10 shows the magnitude of the 1st order filter set to half-power. Equation 4.11 demonstrates the cutoff frequency. The resistor value in the filter is less than 1 kΩ to minimize voltage drop across R_{17}. Equation 4.12 shows the phase of the 1st order filter calculated in degrees. Figure 4.7 demonstrates the simulated bode plot of the passive lowpass filter.

$$H(s) = \frac{1}{sC_{33}R_{17} + 1} \tag{4.9}$$

$$|H(\omega)| = \frac{1}{\sqrt{(C_{33}R_{17}\omega)^2 + 1}} = \frac{1}{\sqrt{2}} \tag{4.10}$$

$$f_c = \frac{\omega_c}{2\pi} = \frac{1}{2\pi} * \frac{1}{C_{33}R_{17}} = \ 1.59 \ MHz \tag{4.11}$$

$$\phi = \angle H\left(\omega\right) = -\frac{180\ ^\circ}{\pi} * tan^{-1}\left(\omega C_{33}R_{17}\right) \tag{4.12}$$

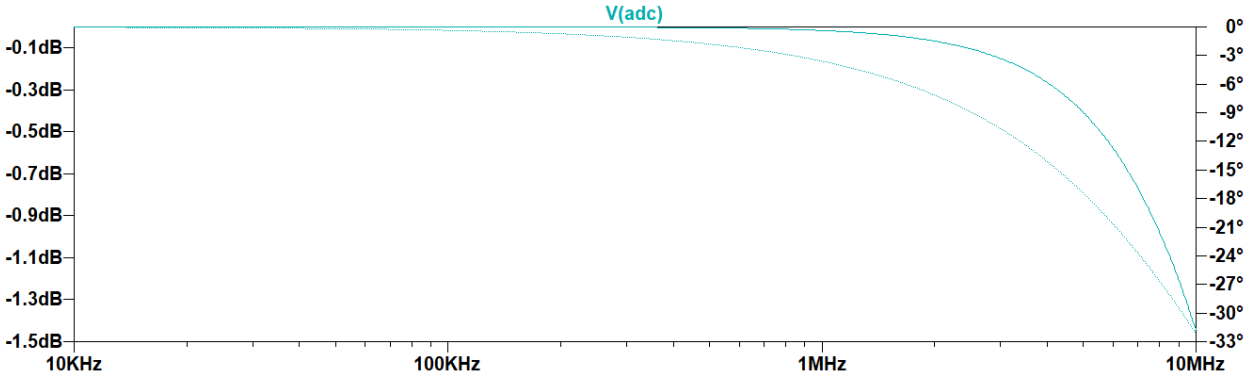

Figure 4.7: 1st Order Lowpass Filter Bode Simulation

Quantization noise derives from the signal-to-noise ratio as a function of the number of bits that the ADC samples as shown in Equation 4.13.

$$SNR_{\max} = 6.02N + 1.76 = 6.02\left(16\right) + 1.76 \approx 98 \ dB \tag{4.13}$$

4.4 Digital-to-Analog Converter

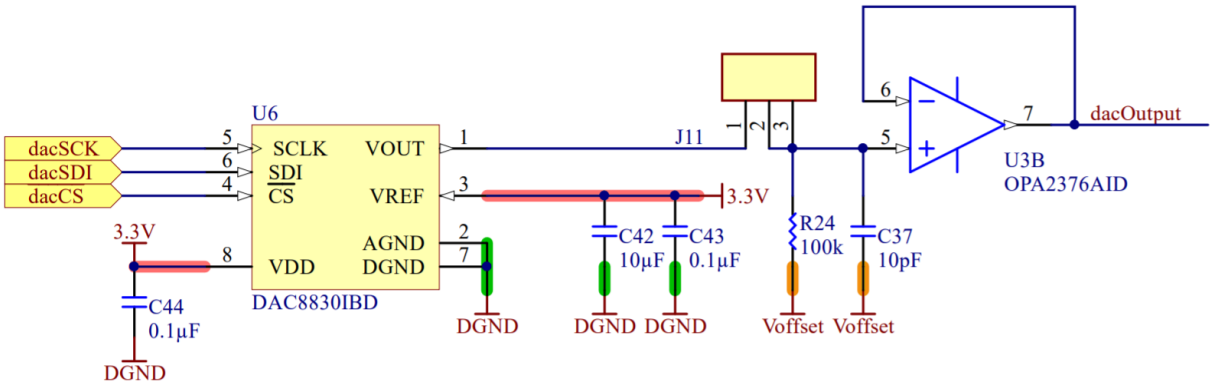

Figure 4.8: Digital-to-Analog Converter Circuit

The DAC8830 chip is a 16-bit DAC that accepts the serial input data, clock signal, and chip select from the microcontroller as shown in Figure 4.8. The output of the DAC connects to a resistor divider comprised of a potentiometer and resistor that reference V_{offset}. The potentiometer controls the volume of the processed signal. The amplitude of a signal determines volume. Full volume occurs when the potentiometer is set to 0 Ω. A capacitor connected in parallel with the R_{24} filters high frequencies. The circuit connects to a voltage follower op-amp. The output of the buffer is labeled as dacOutput.

4.5 Summing Circuit

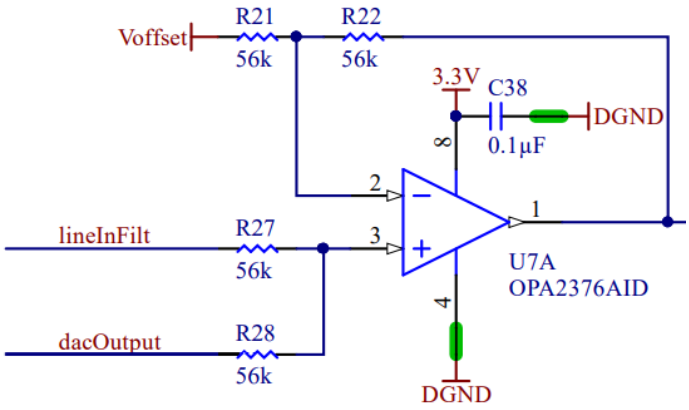

Figure 4.9: Summing Amplifier Circuit

The summing amplifier circuit, shown in Figure 4.9, sums the lineInFilt and dacOutput nodes by use of a non-inverting summing amplifier with 2x gain. The signals sum together with respect to V_{offset} which keeps the audio signal midway between 3.3 V_{DC} and digital ground. Equation 4.14 shows the transfer function of the summing circuit with respect to 1.65 V_{DC}. All resistors are identically sized and dacOutput and lineInFilt are centered at 1.65 V_{DC} to reduce the complexity of the transfer function as shown in Equation 4.15.

$$V_{out} = \left(1 + \frac{R_{22}}{R_{21}}\right) * \left(V_{dacOutput} * \frac{R_{27}}{R_{27} + R_{28}} + V_{lineInFilt} * \frac{R_{28}}{R_{27} + R_{28}}\right) \tag{4.14}$$

$$V_{out} = V_{dacOutput} + V_{lineInFilt} \tag{4.15}$$

Figure 4.10 shows the individual simulated lineInFilt and dacOutput nodes waveforms. Figure 4.11 shows the sum of the two waveforms taken at the output of the summing amplifier.

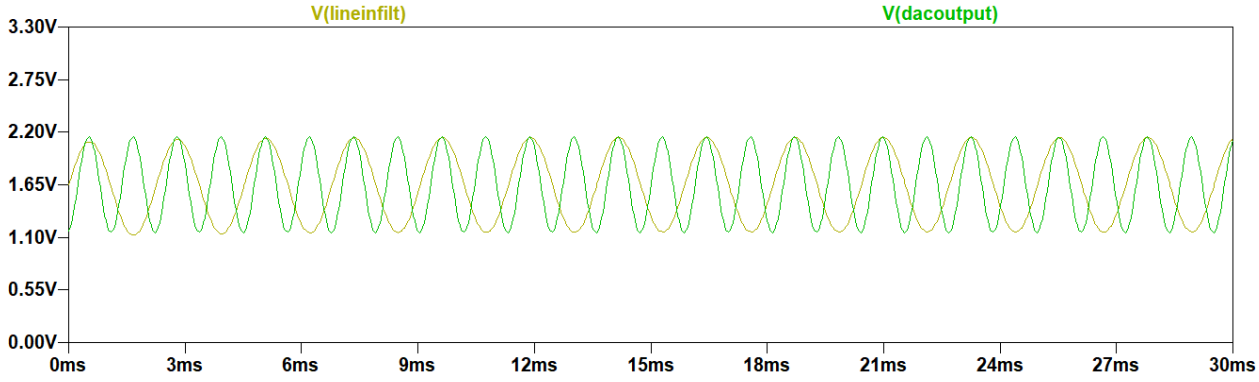

Figure 4.10: LineInFilt (440 Hz) and dacOutput (880 Hz) centered at 1.65 V_{DC}

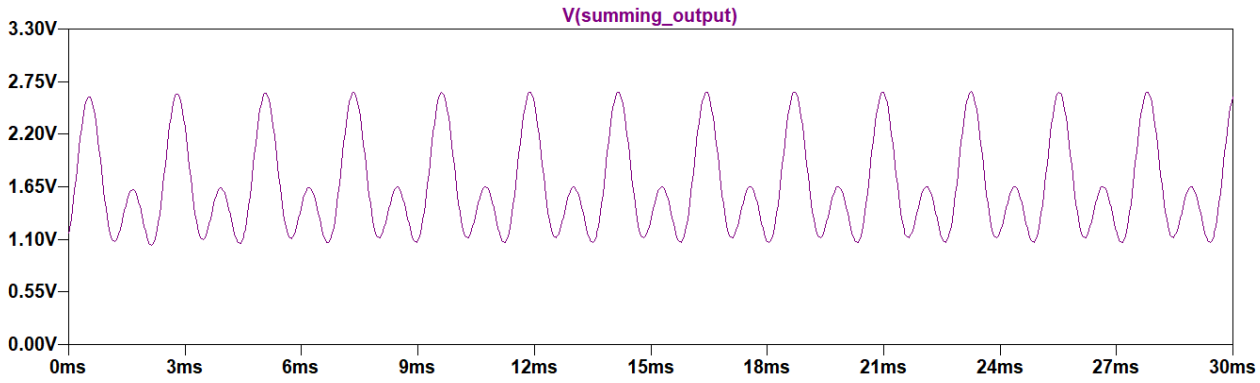

Figure 4.11: Sum of LineInFilt and dacOutput at Output of Summing Circuit

4.6 Output Lowpass Filter

The final stage at the output of the system is a Sallen-Key lowpass filter that blocks frequencies outside the human audible range as shown in Figure 4.12. The output of the amplifier is in series with a coupling capacitor that removes offset voltage. The input impedance of instrument amplifiers, which lineOUT node connects to, is in the range 100 kΩ – 1 MΩ [26].

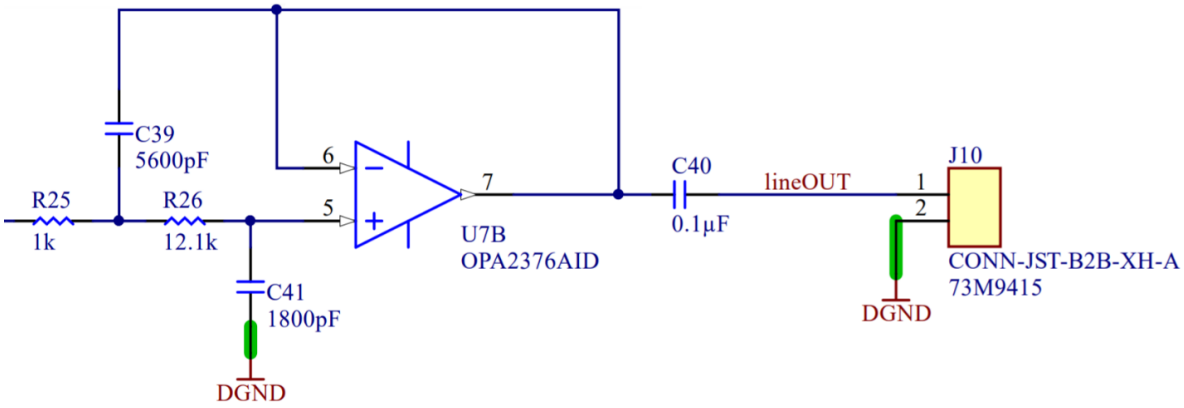

Figure 4.12: Sallen-Key Lowpass Filter

The transfer function of the Sallen-Key filter is shown in Equation 4.16 and re-organized to simplify the derivation of the 2nd order equation variables in Equation 4.17. A Sallen-Key lowpass filter is comparable to two sequential passive 1st order lowpass filters. The design begins by sizing R_{26} at least 10x larger than R_{25} to prevent the second stage (R_{26}-C_{41}) from loading the first stage (R_{25}-C_{39}) and obtain a sharper roll-off at the cutoff region. Similarly, C_{41} is larger than C_{39}. The capacitor values are in the nanofarad region, as opposed to picofarad, to achieve low noise at a tradeoff with low power [27]. The coupling capacitor has a value of at least 0.1 µF to prevent any unintended highpass filtering of the lower frequencies in the audible range.

$$H(s) = \frac{1}{s^2 R_{25}R_{26}C_{39}C_{41} + (R_{25}C_{41} + R_{26}C_{41})s + 1} \tag{4.16}$$

$$H(s) = \frac{\omega_o^2}{s^2 + \frac{\omega_o}{Q}s + \omega_o^2} = \frac{\frac{1}{R_{25}R_{26}C_{39}C_{41}}}{s^2 + \left(\frac{1}{R_{26}C_{39}} + \frac{1}{R_{25}C_{39}}\right)s + \frac{1}{R_{25}R_{26}C_{39}C_{41}}} \tag{4.17}$$

An effective filter has a steep cutoff region which occurs with a higher quality factor. However, a quality factor of $Q < 0.5$ and damping ratio $\zeta > 1$ are necessary to prevent the system from becoming underdamped which creates self-oscillations. The RC values of the Sallen-Key filter give a quality factor of $Q = 0.468$ as shown in Equation 4.18 and a damping ratio of $\zeta = 1.067$ as shown in Equation 4.19. These Q and ζ values yield a steep cutoff region while keeping the filter overdamped.

$$Q = \frac{\sqrt{R_{25}R_{26}C_{39}C_{41}}}{C_{41}(R_{25} + R_{26})} = 0.468 \tag{4.18}$$

$$\zeta = \frac{1}{2Q} = 1.067 \tag{4.19}$$

The calculation for the natural frequency is shown in Equation 4.20. The consequence of a system where $Q \neq \frac{1}{\sqrt{2}}$ is that the natural frequency shifts away from the half-power point as a function of Q as seen in Equation 4.21.

$$f_n = \frac{\omega_o}{2\pi} = \frac{1}{2\pi} * \frac{1}{\sqrt{R_{25}R_{26}C_{39}C_{41}}} = 14.411\ kHz \tag{4.20}$$

$$|H(\omega_o)| = 20 * \log_{10}(Q) = -6.588\ dB \tag{4.21}$$

To find the frequency of the half-power point, the damping ratio is taken into account as shown in Equation 4.22 (see Appendix A for a full derivation). Equation 4.23 shows the phase of the filter calculated in degrees. Figure 4.13 shows a simulated bode plot of the output Sallen-Key lowpass filter.

$$f_{-3dB} = f_n * \sqrt{1 - 2\zeta^2 + \sqrt{4\zeta^4 - 4\zeta^2 + 2}} = 8.459\ kHz \tag{4.22}$$

$$\phi = \angle H(\omega) = -\frac{180\ ^\circ}{\pi}\left(tan^{-1}\left(\frac{2\zeta\omega\omega_o}{\omega_o^2 - \omega^2}\right)\right) \tag{4.23}$$

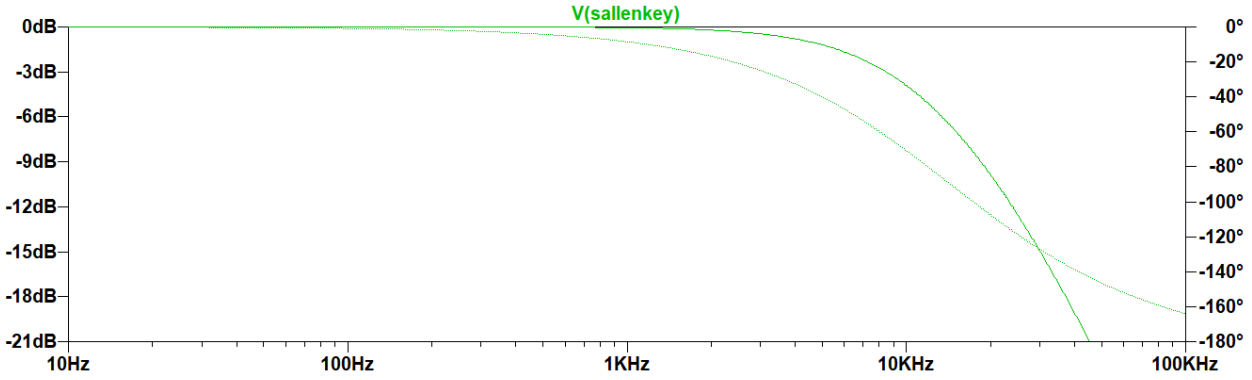

Figure 4.13: Bode Plot Simulation of Sallen-Key Lowpass Filter

4.7 Noise Simulation

There are two types of noise associated with resistors: thermal noise and excess noise, which is discussed in Section 5.2. Thermal noise of resistors is a function of Boltzmann's constant, temperature, resistance, and bandwidth as demonstrated by Equation 4.24.

$$v_n = \sqrt{4k_B T R \Delta f} \tag{4.24}$$

Thermal noise is 'white' since it has the capacity to generate equal energy at every frequency [28]. Ideal capacitors do not generate noise in isolation. However, a capacitor shapes the noise of a 1^{st} order RC circuit which alters the equation for thermal noise as seen in Equation 4.25 which is a function of capacitance, temperature, and Boltzmann's constant.

$$v_n = \sqrt{\frac{k_B T}{C}} \tag{4.25}$$

Per Equations 4.24 and 4.25, thermal noise is directly proportional to resistance and inversely proportional to capacitance. It is beneficial to pick lower resistor values (in the kΩ region) and higher capacitor values (in the nanofarad region). Figure 4.14 is a noise simulation of the system in its entirety. An integrated value of the plot gives an estimate of $v_n = 7.7432\ \mu V_{RMS}$ in the audible range from 20 Hz to 20 kHz.

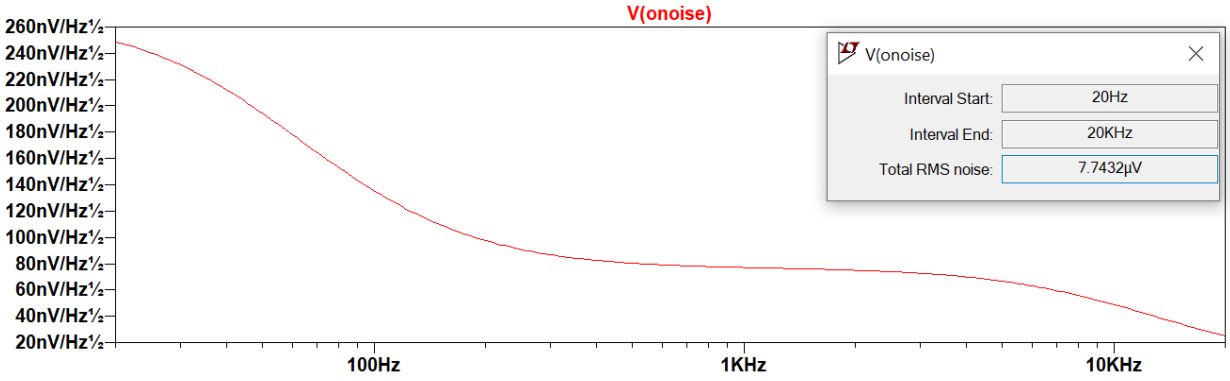

Figure 4.14: Noise Simulation of Loop Pedal Circuit

4.8 Microcontroller

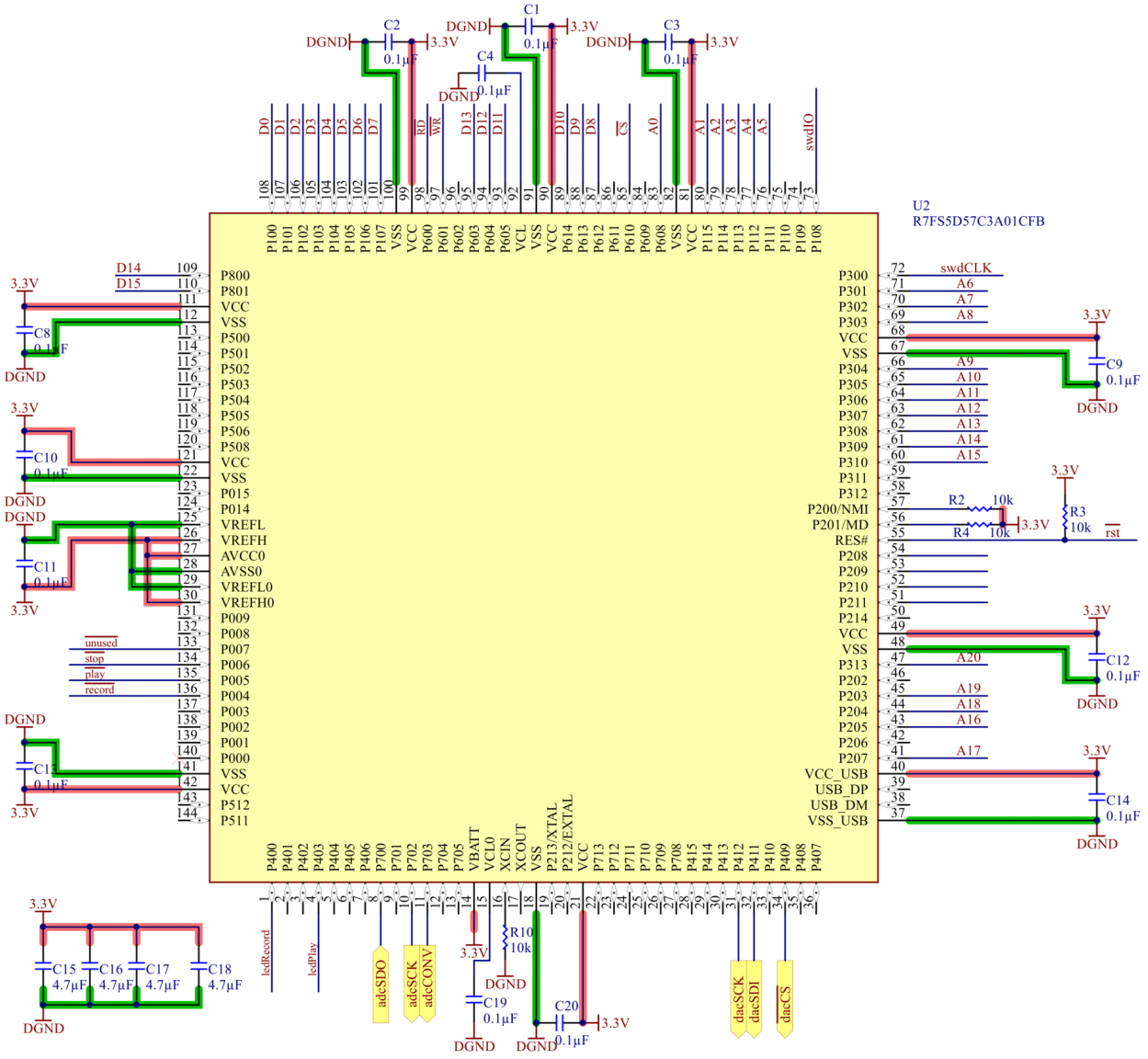

Figure 4.15: Microcontroller Schematic

The microcontroller, shown in Figure 4.15, controls four modules: ADC, DAC, system memory, and the LED circuit. During the 'record' state the microcontroller writes the serial data from the ADC to the system memory sequentially, writing the bits in parallel, until the user places the system in the 'play' state or until the memory is full. The microcontroller turns on a red LED during the 'record' state. During the 'play' state, the microcontroller reads the data in the system memory, reading the bits in parallel, and outputs it to the DAC as serial data. The microcontroller turns on a green LED during the 'play' state. The microcontroller is programmed with an SWD (Serial Wire Debug) connector as shown in Figure 4.16.

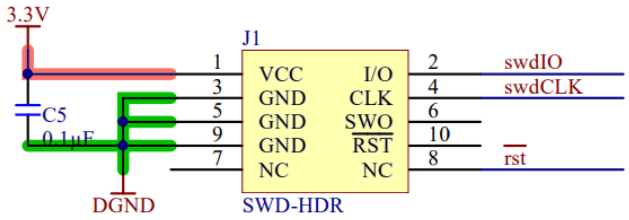

Figure 4.16: SWD Connector Pins on PCB

The system is either in the 'play' state or the 'record' state. The user puts the microcontroller in each state with an SPST footswitch that either grounds or floats the record or play signal to the microcontroller. The signals are set to 3.3 V_{DC} with a pull-up resistor. A second switch clears the system memory and places the system in the turn-on state. Diodes are in series with the center node connected to each signal to clamp the voltage and prevent any damage to the GPIO (General-Purpose-Input-Output) pins of the microcontroller. The switch circuit is shown in Figure 4.17.

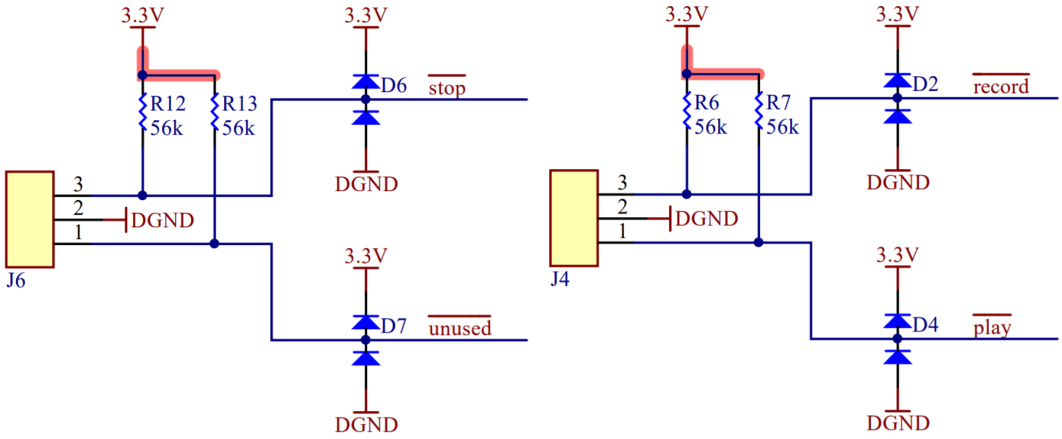

Figure 4.17: Switch Circuit to Control State of System

4.9 System Memory

The system memory, shown in Figure 4.18, uses a CY62167DV30LL SRAM capable of holding 10^6 of 16-bit addresses. The $\overline{\text{BHE}}$ (Byte High Enable), $\overline{\text{BLE}}$ (Byte Low Enable), and V_{SS} pins connect to digital ground, the $\overline{\text{BYTE}}$ (Byte Enable) and CE_2 (Chip Enable 2) connect to 3.3 V_{DC}, and the $\overline{\text{DNU}}$ (Do Not Use) pin floats as indicated in the datasheet. The microcontroller instructs the system to write A_0 to A_{19} to the system memory with the $\overline{\text{WE}}$ (Write Enable) pin and to read D_0 to D_{15} with the $\overline{\text{OE}}$ (Output Enable) pin. The CE_1 (Chip Enable 1) is controlled by the CS (Chip Select) signal from the microcontroller.

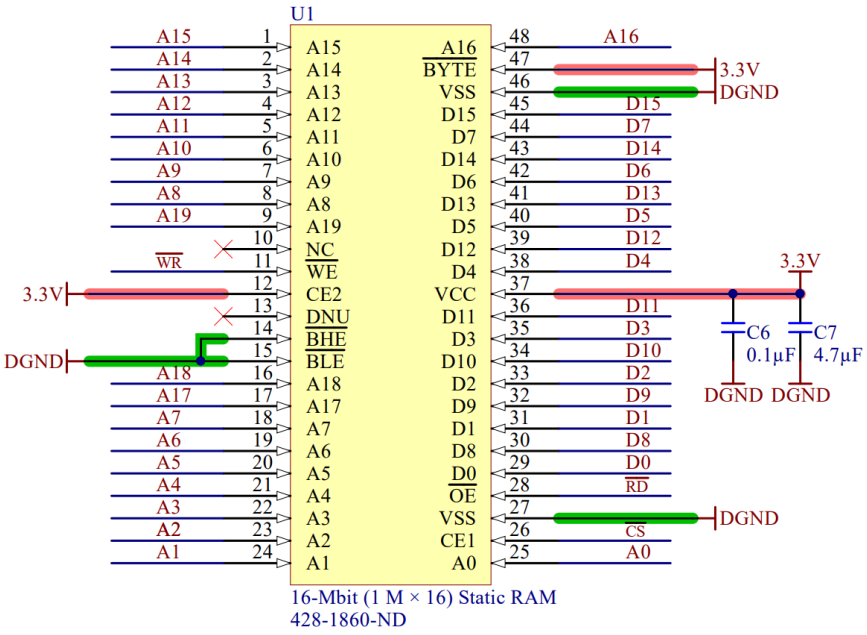

Figure 4.18: System Memory

4.10 LED Circuit

The system has three LEDs that indicate power to the system and state of the system. All LEDs connect to a pull-up resistor which supplies the necessary current for the component to turn on. The yellow LED indicating power to the system turns on when the SPST switch is closed. The green and red LEDs, which indicate whether the system is in 'play' or 'record' state, connect to the drain terminal of an n-channel MOSFET with a grounded source. A voltage signal at the gate from the microcontroller shorts the path from drain-to-source as seen in Figure 4.19.

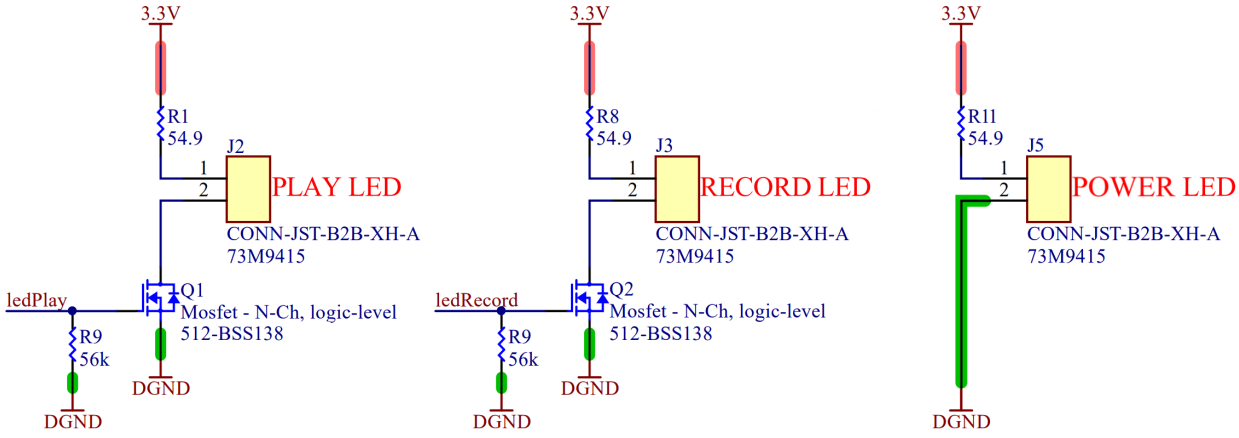

Figure 4.19: Schematic of LED Circuit

4.11 AC Analysis

The frequency response of the comprehensive analog circuit lies between 20 Hz and 20 kHz with a slight gain in the passband region to account for audio losses that occur in system. Figure 4.20 shows the simulated bode plot of the audio output with respect to the audio input.

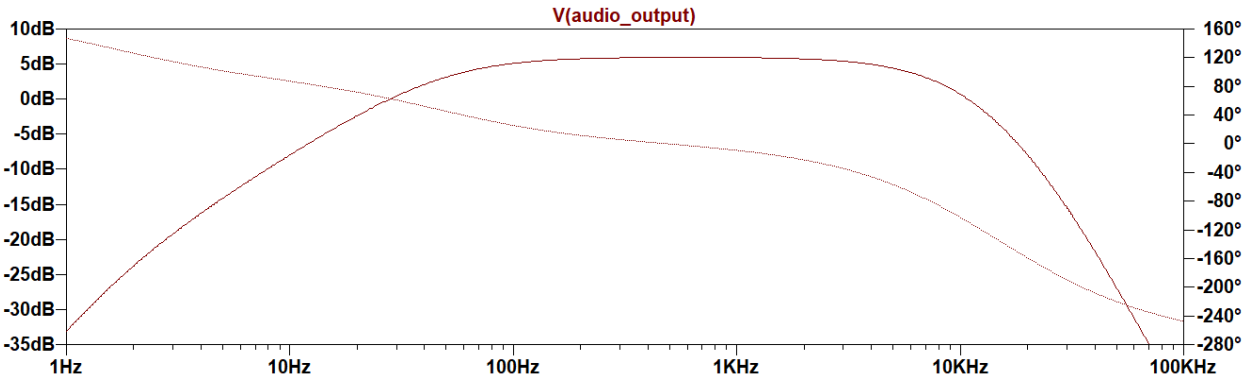

Figure 4.20: Bode Plot Simulation of Analog Circuit

Chapter 5

Hardware Tests and Results

In addition to standard component characteristics for electronics – such as package size, tolerance, and power ratings – there are additional considerations to account for in audio design. Temperature coefficients of capacitors and material characteristics of resistors can reduce or increase the noise and distortion in a circuit [29].

5.1 Capacitor Selection

Film capacitors, such as polypropylene and polyethylene, are the ideal choice for audio because they maintain the integrity of an audio signal. However, they are primarily manufactured for through-hole products as opposed to SMD (Surface Mount Device) and are high-cost compared to ceramic capacitors. MLCC's (Multilayer Ceramic Capacitors) are low-cost and are manufactured in small package sizes. Unfortunately, ceramic capacitors exhibit piezoelectric effects which amplify noise and create variations in the signal path [30]. Class II ceramic capacitors are readily available in a wide range of package sizes and values due to their high permittivity. This availability comes at a tradeoff of decreased performance. Applying time-based voltages to Class II ceramic capacitors produce distortion which prominently manifests in the human audible range. Additionally, because of their high permittivity, Class II capacitors degrade with temperature, usage, and applied voltage as seen in Figure 5.1. Class I capacitors, such as C0G/NP0, have lower permittivity and less of the problems that plague their Class II counterparts, such as X7R. The tradeoff of lower permittivity is that Class I capacitors are not as readily accessible in value and package size.

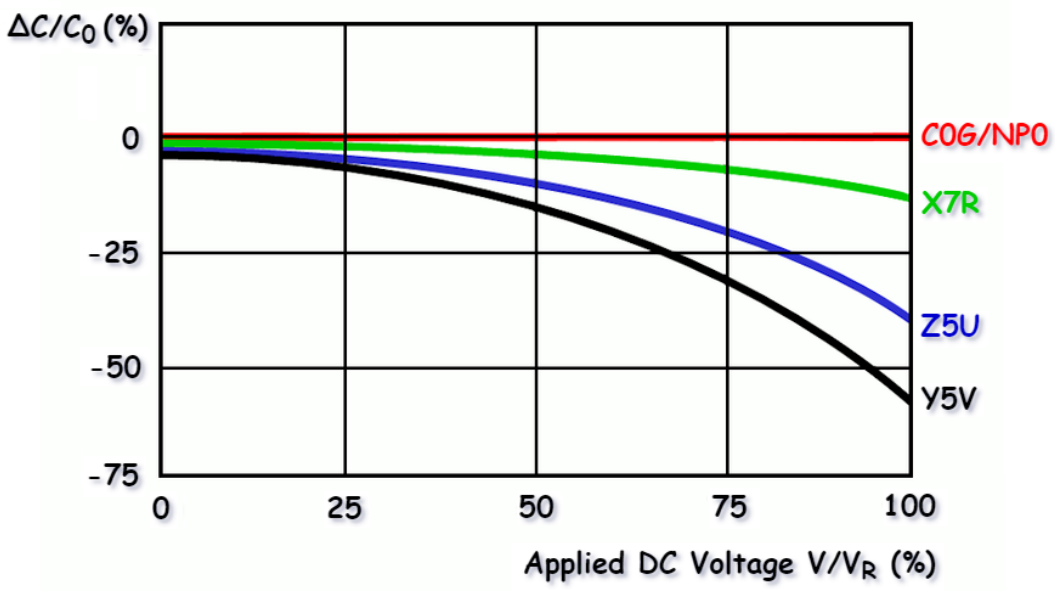

Figure 5.1: Class I (C0G/NP0) and Class II (X7R, Y5V, Z5U) Capacitors

To balance cost, availability, and space, this project uses plastic film capacitors for the signal path and Class I (C0G) capacitors elsewhere for values of C < 0.22 µF. For the bypass capacitors with higher values, Class II (X7R) capacitors are necessary [31].

5.2 Resistor Selection

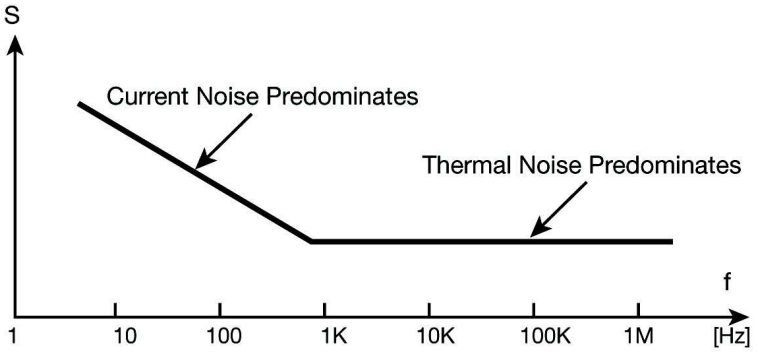

Figure 5.2: Flicker/Thermal Noise vs Resistance Value [32]

Excess noise, sometimes called flicker noise or 1/f noise, is 'pink' since the amplitude of the generated noise is inversely proportional to frequency as seen in Figure 5.2. This phenomenon occurs most prominently as a function of DC voltage and is present across a resistor as shown in Equation 5.1. The equation is dependent on DC voltage, frequency, and constant k, which varies with resistor material.

$$S(V_{nex}) = \frac{k * V_{DC}^2}{f} \tag{5.1}$$

Identically valued resistors from different materials have different noise index as seen in Figure 5.3. Thick-film and carbon composition resistors are low-cost while faring poorly on the flicker noise spectrum. Wirewound resistors are low-noise with high series inductance which cause resonance. Metal foil and thin-film resistors are low-noise and ideal for audio. Of these two, metal foil resistors are superior but can cost nearly 100x a thin-film resistor. At the pursuit of a reasonably low-cost system, this project exclusively uses thin-film resistors [33].

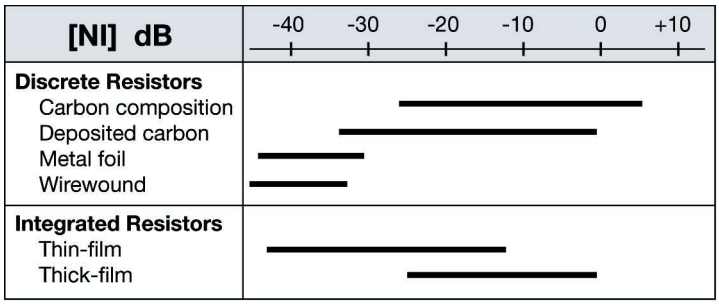

Figure 5.3: Noise Index of Resistors by Component [32]

5.3 Code

The audio signal is sampled at 44.1 kHz to comply with industry standards. A hardware timer available from the Renesas S5D5 ARM Cortex M4 triggers an ISR (Interrupt Service Routine) every 22.67 µs that leads to the system state machine shown in Figure 5.4. The interrupt controls the ADC sampling when recording and controls the DAC when playing back. A detailed list of actions performed during each state is described in Table 5.1.

Figure 5.4: Finite State Machine Diagram

The switch module determines the desired state. A debounce time of 100 ms is set to account for multiple rising edges which prevents a single switch press to execute numerous commands. After the debounce time, a function callback sets a flag for the state machine. A GPIO drives the gate of an n-channel MOSFET that powers the LEDs. A PWM (Pulse-Width Modulator) varies the current at the gate of the MOSFET to reduce power consumption.

Table 5.1: Finite State Machine Actions

State	Actions
Init	Default State on Power-Up Only Executed on Power-Up Initialization on Power-Up Initialize Event Handler Stop ADC Converter Set DAC CS High Disable SPI Modules
Reset	Stop ADC Converter Set DAC CS High Disable SPI Modules Set DAC Output to 0 Initialize SRAM Set Event Handler Reset Flag cmd.bit.reset = false
Play	Set Event Handler Play Flag Transfer SRAM Data to DAC until cmd.b.reset == true OR cmd.b.record == true
Record	Read Data from ADC and Write to SRAM until full Transfer to PLAY State

5.4 Printed Circuit Board Design

The PCB (Printed Circuit Board), shown in Figure 5.5, has four layers: the top and bottom layers for the digital signals, the second layer for ground, and the third layer for V_{CC}. The PCB stackup is organized to have the digital signals on the outer layers, top and bottom, and power path on the inner layers. This architecture places all signal layers next to a power or ground plane so that the current will make a predictable return path. This setup also reduces EMI (Electromagnetic Interference), prevents the return current from coupling inductively or capacitively back to the source, and prevents interference from other signals. Additionally, this architecture places the ground plane directly underneath the processor and SRAM to reduce ground bounce. There is a "keep-out" trace on every layer of the board that encloses the analog signals in an island. This trace also keeps the high-speed digital switching signals from corrupting the sensitive analog data [34].

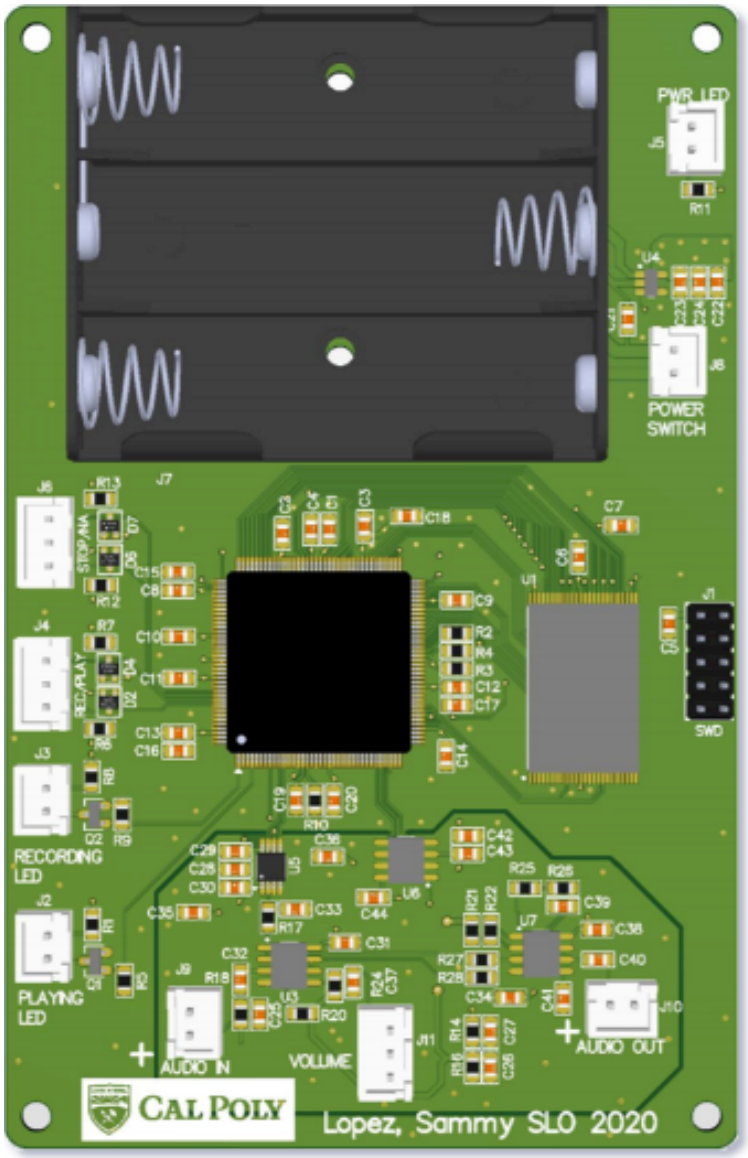

Figure 5.5: Printed Circuit Board

5.5 Measurements

The following are scope images collected from testing the final product with a function generator. The integrity of the audio input signal is maintained throughout the system in a satisfactory manner. Figure 5.6 is an oscilloscope image of the input and output audio signals. The two signals have near identical peak-to-peak voltages and a 3.3° phase difference.

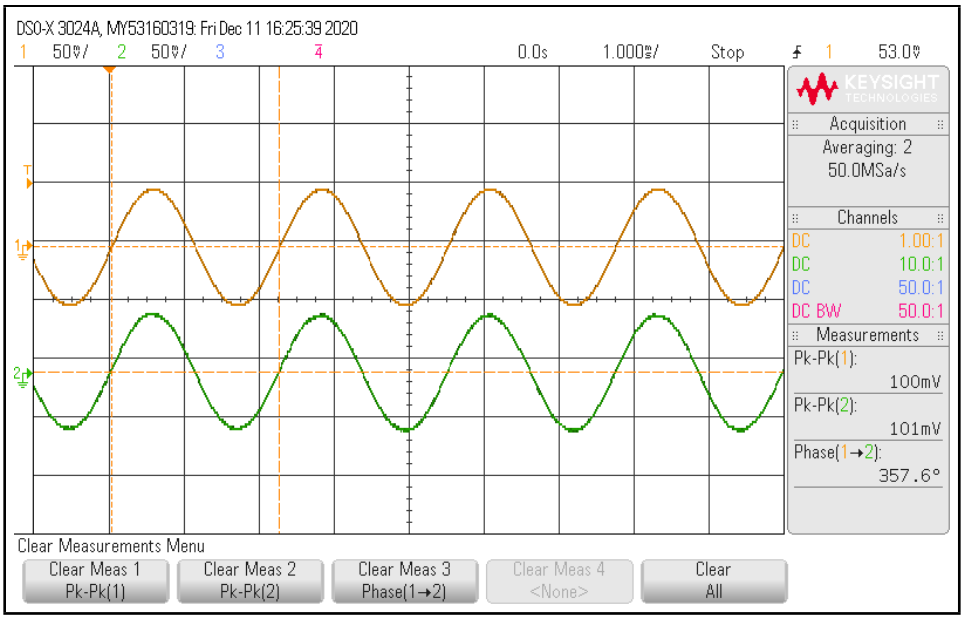

Figure 5.6: CH1 Input Sine Wave & CH2 Output Sine Wave

The integrity of the audio signal is not fully preserved at the output of the digital modules as evidenced in Figure 5.7. Whereas a pure sine wave with a frequency of 440 Hz is generated at the input, there are several disconnects at the output where the sampled signal is broken. The frequency is adequately preserved.

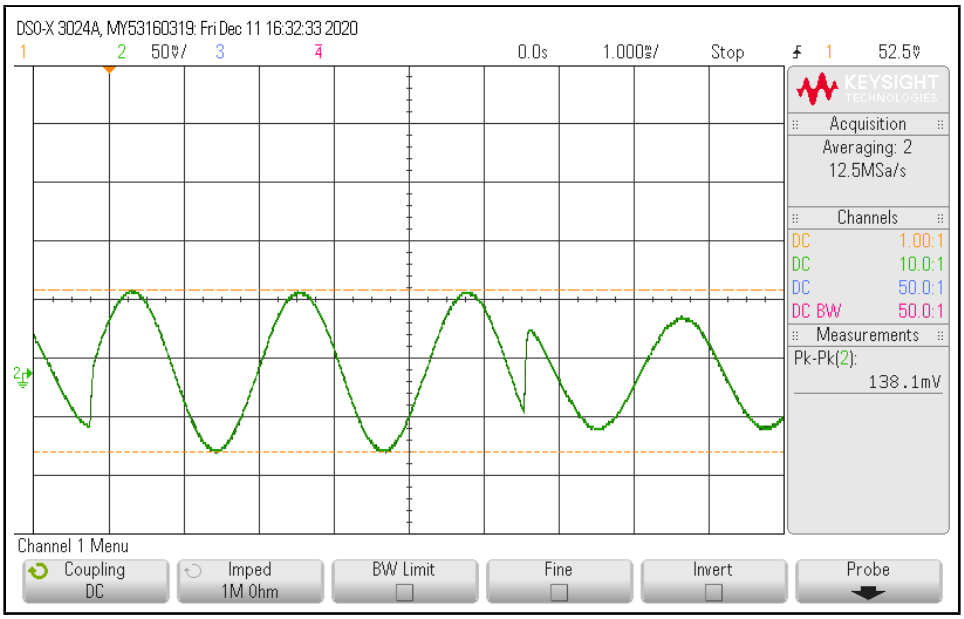

Figure 5.7: CH2 Sampled Sine Wave

Figure 5.8 is a scope image of the output at the summing stage which adds input and processed signals together. The sampled signal is 440 Hz and the audio input signal is 880 Hz which tests the summing stage with different frequencies.

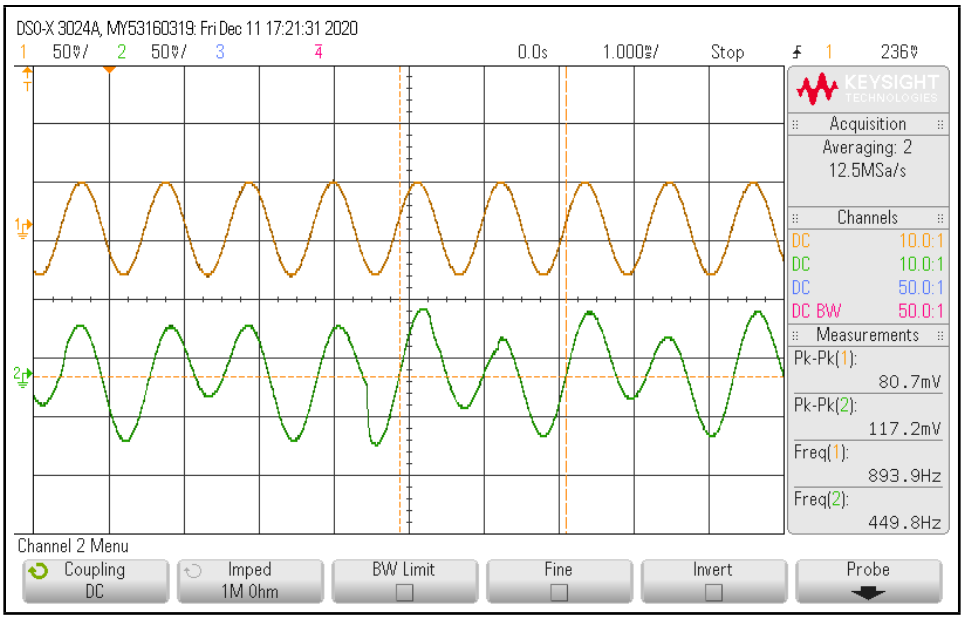

Figure 5.8: CH1 Input Sine Wave & CH2 Input Sine Wave + Sampled Signal

A detail that cannot be captured on a scope image is variance in peak-to-peak voltage of the audio input signal which continuously shifts between 50 mV and 120 mV. This phenomenon occurs when the input signal connects to the system. This may indicate that the analog and digital grounds are not appropriately tied together on the PCB.

The frequency response is measured with a network analyzer when the system is powered on with no input or sampled signal as shown in Figure 5.9. The roll off begins at 8.032 kHz which is consistent with Equation 4.22.

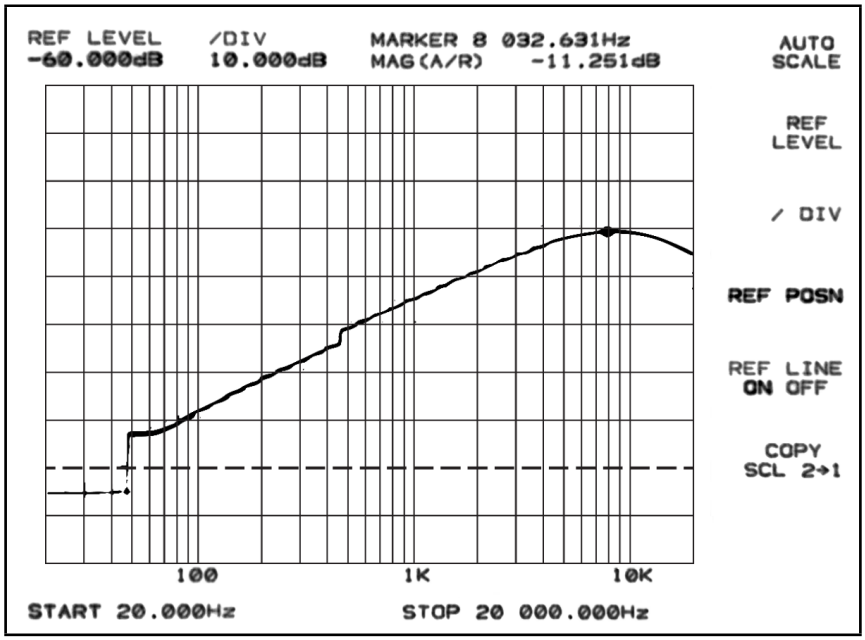

Figure 5.9: Frequency Response Measured by Network Analyzer

5.6 Efficiency

The input voltage and current are measured in parallel and in series, respectively, with the 4.5 V_{DC} power supply. As all integrated chips are powered by 3.3 V_{DC}, the output voltage and current are measured in parallel and in series, respectively, at the output of the LDO. The efficiency of the LDO is limited by the values of the input and output voltages as shown in Table 5.2.

Table 5.2: Efficiency of Power Supply

	Input	Output
Voltage (V)	4.429	3.298
Current (mA)	44.30	44.12
Power (mW)	196.2	145.5
Efficiency	74.2%	

A single alkaline AA battery is rated at 1.5 V_{DC} for 1500-2400 mA/hours. At a lower bound, the system has a time of playability on three AA batteries as shown in Equation 5.2 [35].

$$Time\ of\ use = \frac{1500\ mA * hours}{1.5\ V_{DC}\ battery} * \frac{3 * (1.5\ V_{DC}\ battery)}{44.3\ mA} \approx 102\ hours \tag{5.2}$$

5.7 Audible Analysis

The output audio signal of the system is audibly consistent with the analog input, as shown in Figure 5.4. The frequency response is slightly different than expected which may be due to gain and filtering deviations. There are two undesired anomalies that may hinder future production of these units. A high frequency hissing sound is ever present that increases in intensity when the finite-state machine is in the 'play' state after a signal has already been sampled. As previously stated, this may be due to the analog and digital grounds not being appropriately tied. There is a break in the audio that leads to an audibly noticeable loss of approximately 100 ms worth of signal. This loss of signal inexorably yields unsatisfactory recorded audio. Whether this glitch occurs when the finite-state machine changes from 'play' to 'record' or from 'record' to 'play' is unclear.

Chapter 6

Future Improvements

The primary goal of this project was to create an electronic device that could sample an analog audio signal, store it digitally, and recreate the stored data. This device allows for a recorded signal to be superimposed in real-time with a live audio signal. While this task was completed, there are several possible improvements for future iterations of this project.

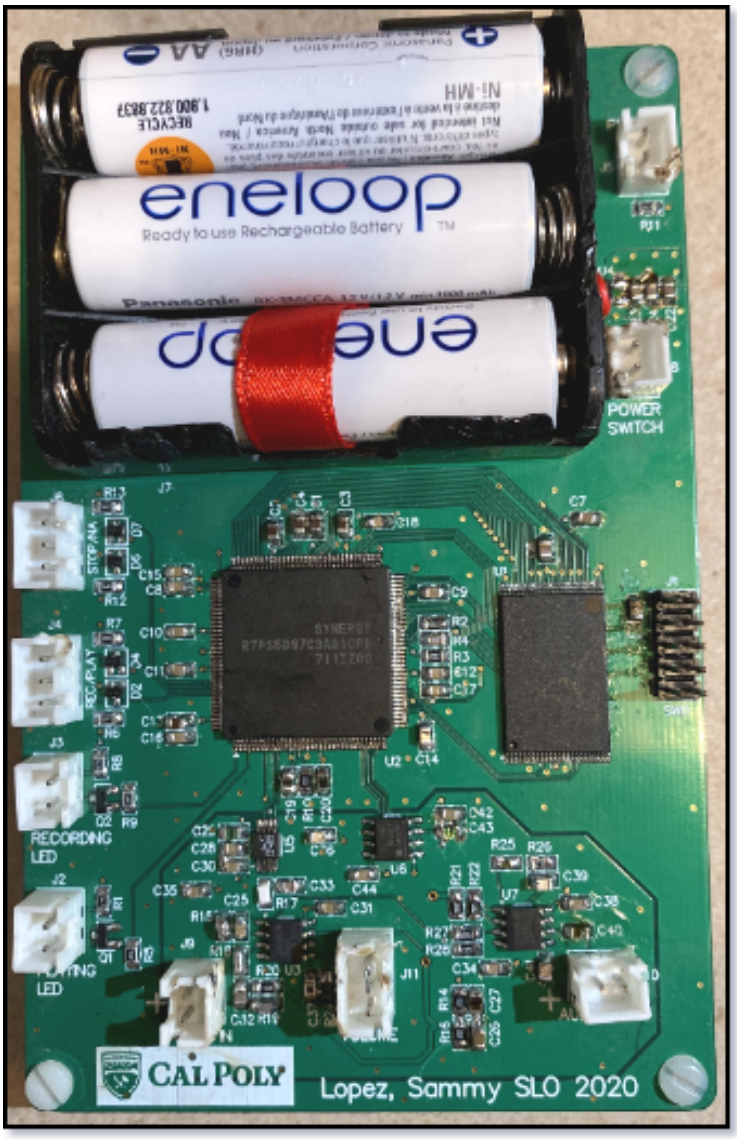

Figure 6.1: Audio Loop Station PCB

6.1 Power Supply

Using three AA batteries for the power supply is space-consuming as shown in Figure 6.1. Changing the power supply to a 9 V_{DC} battery will match industry standards albeit at the cost of higher power consumption. Centering the audio signal at an offset voltage using resistors is non-ideal and power-consuming. An LDO with two outputs, one for power and one for offset, is a better choice for future versions of this project. The ground connection between analog and digital signals is noisy and wavers irregularly. Additional research is necessary to implement a stabler signal.

6.2 Analog Signals

The amplitude of an audio signal varies depending on user, instrument, and intensity of play. The input may see a 100 $mV_{p\text{-}p}$ during light play and 1.0 $V_{p\text{-}p}$ during heavy play. This means that signals with lower volume occupy less bits than those with higher volume. This results in lower resolution for lower signals which means that not every signal is sampled equally. Increasing the bit length from 16 bits to 24 bits or higher would ameliorate this issue. The input impedance will be increased with a buffer as is a common practice in the audio industry.

6.3 Firmware

There is a delay between pressing the record switch and the start time of recording audio. Though delays less than 30 ms generally go unnoticed by musicians, in the industry the maximum acceptable delay is 2 ms. Thus, additional steps to reduce the present delay are necessary. The initial ambition of this project included the option of recording and layering multiple audio signals. At present, the pedal records only one track meaning a feedback mechanism is necessary to layer multiple signals. This can be implemented if the firmware continuously sums the digital signals. Adding the option of audio effects – reverb, chorus, distortion – will make the pedal a multi-feature product.

6.4 Hardware

An improvement to this project in a future iteration is to reduce size. The enclosure of the system is larger than a typical loop station as shown in Figure 6.2. A single audio codec could replace the ADC – DAC pair. The passive components can be reduced in size from 0805 to 0201. Upgrading to a single 9 V_{DC} battery will eliminate the need for three AA batteries. Additionally, decreasing the size of the PCB will reduce manufacturing costs.

Figure 6.2: Enclosure for Loop Pedal

6.5 Cost

As seen in the Bill of Materials in Table B.1, the cost of producing one unit is over a hundred dollars. Low priced loop pedals are priced from fifty to a hundred dollars. If this pedal is mass-produced, several adjustments are necessary to make this endeavor financially feasible. Conversely, components are priced at lower cost when purchasing in bulk.

6.6 Final Thoughts

I began my educational journey as a college student enrolled as a music major. As an engineering major I developed an interest in analog circuts. It gives me great pleasure that all these years later I could combine my love for music and my passion for circuits. The scope of this project is bigger than anything I'd previously attempted as it contains elements of power electronics, analog design, embedded systems, firmware, and PCB design. Being able to assemble so many independent modules into a single audio device is the most rewarding experience I've had as an engineer.

Bibliography

[1] M. Cochran and L. Paul. *Les Paul in His Own Words*. Backbeat Books, 2016. ISBN: 9781495047398.

[2] Les Paul. *The Inventions*. http://www.les-paul.com/timeline/les-the-inventor/. 2020.

[3] D. Hunter. *Guitar Effects Pedals: The Practical Handbook*. HANDBOOK SERIES. Hal Leonard, 2013. ISBN: 9781617131011.

[4] Alaina G. Levine. *Bell Telephone Laboratories, New Jersey*. https://www.aps.org/programs/outreach/history/historicsites/transistor.cfm. 2008.

[5] A. Thompson. *The Stompbox*. G - Reference, Information and Interdisciplinary Subjects Series. Miller Freeman Books, 1997. ISBN: 9780879304799.

[6] Janies Insola and Henry Rasof. *Electronic Projects for Musicians*. Amsco Publications, 1975.

[7] Thomas Fine and Barry R. Ashpole. *The Dawn of Commercial Digital Recording*. http://www.aes.org/aeshc/pdf/fine_dawn-of-digital.pdf. 2020.

[8] Oberheim. *1994 Catalog*. http://www.livelooping.org/wp-content/uploads/2018/12/1994-Oberheim-catalog.pdf. 1994.

[9] Kristof Neyens. *Guitar Looping: The Creative Guide*. http://www.fundamental-changes.comwww.fundamental-changes.com. 2019.

[10] M. Grob. *Live Looping - History and Concepts*. http://www.livelooping.org/history_concepts/. 2020.

[11] Bee Suan Ong and Sebastian Streich. "Music loop extraction from digital audio signals". In: *2008 IEEE International Conference on Multimedia and Expo*. IEEE. 2008, pp. 681–684.

[12] Yongwei Zhu, Hui Li Tan, and Susanto Rahardja. "Drum loop pattern extraction from polyphonic music audio". In: *2009 IEEE International Conference on Multimedia and Expo*. IEEE. 2009, pp. 482–485.

[13] Steven W Smith. "Audio Processing". In: *The Scientist and Engineer's Guide to Digital Signal Processing*. California Technical Publishing, 1997, pp. 357–359.

[14] Kun Lin et al. "Digital filters for high performance audio Delta-Sigma analog-to-digital and digital-to-analog conversions". In: *Proceedings of Third International Conference on Signal Processing (ICSP'96)*. Vol. 1. IEEE. 1996, pp. 59–63.

[15] Roy Pines Sallen and Edwin L Key. "A practical method of designing RC active filters". In: *IRE Transactions on Circuit Theory* 2.1 (1955), pp. 74–85.

[16] Vishay. *Creating a Negative Output Voltage Using a Buck Converter*. Document Number 76946. 2016.

[17] Boss. *RC-505 Loop Station: Owner's Manual*. 2003.

[18] Emil Torick. *AES Standard*. www.aes.org/publications/standards/search.cfm?docID=14. 2003.

[19] Andy McFadden. *Why 44.1KHz? Why Not 48KHz?* stason.org/TULARC/pc/cd-recordable/2-35-Why-44-1KHz-Why-not-48KHz.html. 2001.

[20] *LP5907 250-mA, Ultra-Low-Noise, Low-IQ LDO*. SNVS798O datasheet. 2012.

[21] *OPAx376 Low-Noise, Low Quiescent Current, Precision Operational Amplifier e-trim Series*. SBOS406G datasheet. 2015.

[22] *LTC1864L/LTC1865L µPower, 16-Bit, 250ksps 1- and 2-Channel ADCs in MSOP*. LTC1864L CMS8#PBF datasheet. 2007.

[23] *DAC8830IBD 16-Bit, Ultra-Low Power, Voltage-Output Digital-to-Analog Converters*. SLAS449D datasheet. 2007.

[24] *S5D5 Microcontroller Group*. R01DS0317EU0130 datasheet. 2017.

[25] *CY62167DV30 MoBL®16-Mbit (1 M × 16) Static RAM*. Document Number: 38-05328 Rev. *M. 2014.

[26] Fender. *Hot Rod Deville: Reference and Owner's Manual*. P/N 050393.

[27] analog.com. *Filter Design Tool — Filter Wizard — Analog Devices*. https://tools.analog.com/en/filterwizard/. 2020.

[28] Felix Zandman, Paul-René Simon, and Joseph Szwarc. *Resistor theory and technology*. SciTech, 2002.

[29] Zak Kaye. "Selecting capacitors to minimize distortion in audio applications". In: *Analog Design Journal* (2020).

[30] Kemet. *Here's What Make MLCC Dielectrics Different*. https://ec.kemet.com/blog/mlcc-dielectric-differences/. 2020.

[31] Cletus J Kaiser. "The Capacitor Handbook A Comprehensive Guide For Correct Component Selection In All Circuit Applications". In: *CJ Publishing* 2 (1995), p. 77.

[32] Gabriel Vasilescu. *Electronic noise and interfering signals: principles and applications*. Springer Science & Business Media, 2006.

[33] C.J. Kaiser. *The Resistor Handbook*. The passive trilogy. CJ Pub., 1998. ISBN: 9780962852558.

[34] Texas Intruments. "High-speed Interface layout guidelines". In: *Application Report SPRAAR7G-August2014* (2017).

[35] Energizer Energizer. "Lithium Iron Disulfide Handbook and Application Manual". In: (2009).

Appendix A

Derivation of Sallen-Key Lowpass Filter

A.1 Introduction

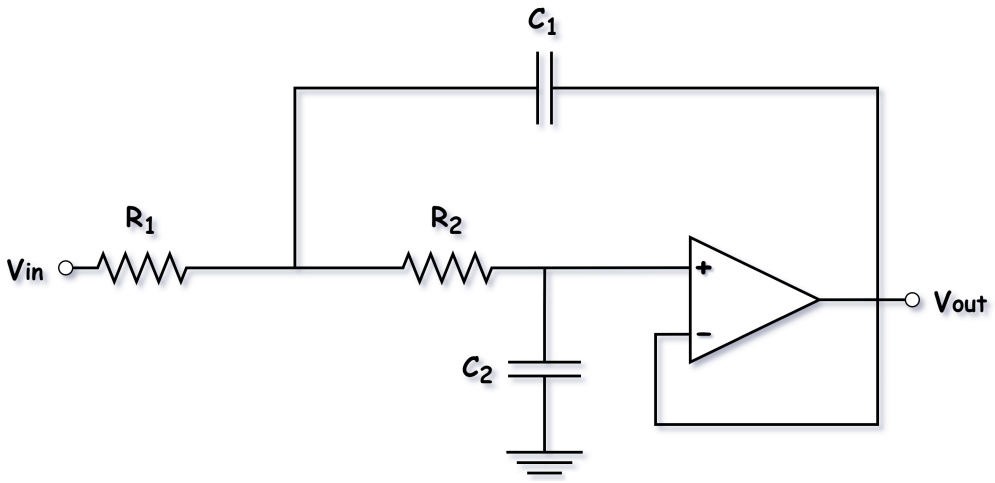

Figure A.1: Sallen-Key Lowpass Filter

A Sallen-Key lowpass filter, shown in Figure A.1, gives a 2nd order equation. If the quality factor is not $Q = \frac{1}{\sqrt{2}}$, then the corner frequency is no longer equal to the natural frequency. Thus, the location of the corner frequency and the magnitude of the natural frequency vary as the quality factor changes as shown in Figure A.2.

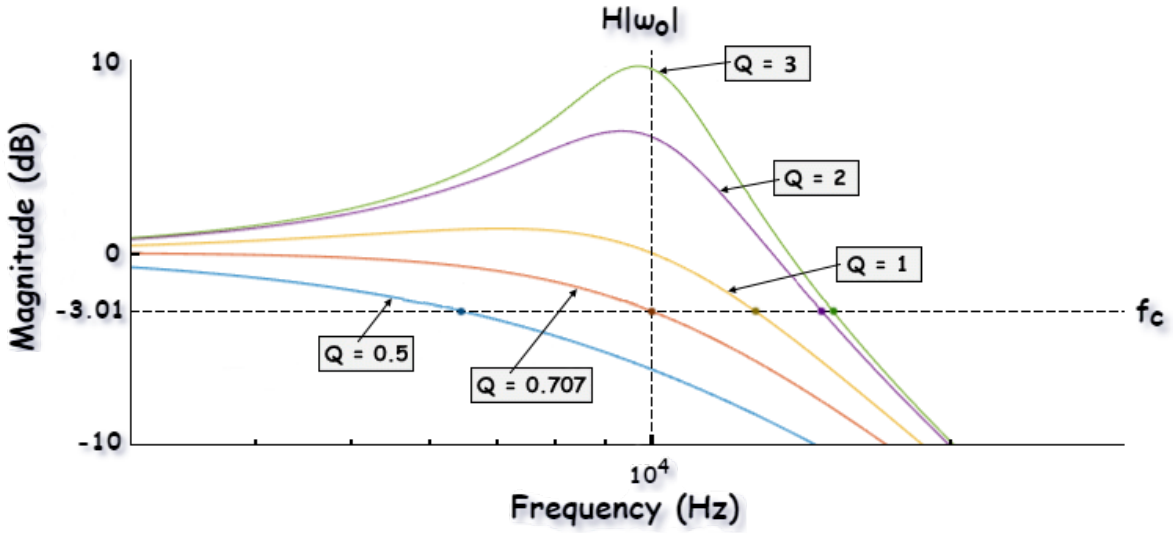

Figure A.2: Frequency Response of 2nd Order Lowpass Filter with Varying Q Factors

A.2 Transfer Function and Key Variables

The derivation for the magnitude of the natural frequency f_n and shifted half-power frequency f_c of a 2nd order Sallen-Key filter with unity gain is as follows. The transfer function of the Sallen-Key lowpass filter is:

$$H(s) = \frac{1}{s^2 R_1 R_2 C_1 C_2 + C_2(R_1 + R_2)s + 1} \tag{A.1}$$

Which can be re-arranged to produce easily derived variables:

$$H(s) = \frac{\omega_o^2}{s^2 + \frac{\omega_o}{Q}s + \omega_o^2} = \frac{\frac{1}{R_1 R_2 C_1 C_2}}{s^2 + \left(\frac{1}{R_1 C_1} + \frac{1}{R_2 C_1}\right)s + \frac{1}{R_1 R_2 C_1 C_2}} \tag{A.2}$$

The natural frequency f_n for a 2nd order lowpass filter can be universally found by the following equations:

$$\omega_o = \sqrt{\frac{1}{R_1 C_1 R_2 C_2}} \tag{A.3}$$

$$f_n = \frac{\omega_o}{2\pi} = \frac{1}{2\pi} * \sqrt{\frac{1}{R_1 C_1 R_2 C_2}} \tag{A.4}$$

The quality factor Q and damping ratio ζ can be calculated as:

$$\zeta = \frac{1}{2Q} \tag{A.5}$$

$$\frac{\omega_o}{Q} = 2\zeta\omega_o = \left(\frac{1}{R_1 C_1} + \frac{1}{R_2 C_1}\right) \tag{A.6}$$

$$Q = \omega_o \div \frac{\omega_o}{Q} = \sqrt{\frac{1}{R_1 C_1 R_2 C_2}} \div \left(\frac{1}{R_1 C_1} + \frac{1}{R_2 C_1}\right) = \frac{\sqrt{R_1 C_1 R_2 C_2}}{C_2(R_1 + R_2)} \tag{A.7}$$

The magnitude of the natural frequency can be calculated by accounting for the quality factor:

$$|H(\omega_o)| = 20 * \log(Q) \tag{A.8}$$

A.3 Corner Frequency and Phase

Transform from Laplace to Fourier:

$$H(j\omega)|_{s=j\omega} = \frac{\omega_o^2}{-\omega^2 + 2\zeta\omega_o j\omega + \omega_o^2} \tag{A.9}$$

The complex conjugate of the denominator:

$$(\omega_o^2 - \omega^2) + 2\zeta\omega_o j\omega \tag{A.10}$$

Is:

$$(\omega_o^2 - \omega^2) - 2\zeta\omega_o j\omega \tag{A.11}$$

To get the real and imaginary parts of the transfer function, multiply numerator and denominator by complex conjugate:

$$H(j\omega) = \frac{\omega_o^2}{(\omega_o^2 - \omega^2) + 2\zeta\omega_o j\omega} * \frac{(\omega_o^2 - \omega^2) - 2\zeta\omega_o j\omega}{(\omega_o^2 - \omega^2) - 2\zeta\omega_o j\omega} \tag{A.12}$$

$$H(j\omega) = \frac{\omega_o^2(\omega_o^2 - \omega^2) - 2\zeta\omega_o^3 j\omega}{(\omega_o^2 - \omega^2)^2 \ + \ 4\zeta^2\omega_o^2\omega^2} \tag{A.13}$$

Separate the real and imaginary parts:

$$Re(H(j\omega)) = \frac{\omega_o^2(\omega_o^2 - \omega^2)}{(\omega_o^2 - \omega^2)^2 \ + \ 4\zeta^2\omega_o^2\omega^2} \tag{A.14}$$

$$Im(H(j\omega)) = \frac{-2\zeta\omega_o^3\omega}{(\omega_o^2 - \omega^2)^2 \ + \ 4\zeta^2\omega_o^2\omega^2} \tag{A.15}$$

To find magnitude, take the square root of the sum of the real and imaginary parts of the transfer function:

$$|H(j\omega)| = \sqrt{Re(H(j\omega))^2 + Im(H(j\omega))^2} \tag{A.16}$$

$$Re(H(j\omega))^2 = \frac{\omega_o^4(\omega_o^2 - \omega^2)^2}{((\omega_o^2 - \omega^2)^2 \ + \ 4\zeta^2\omega_o^2\omega^2)^2} \tag{A.17}$$

$$Im(H(j\omega))^2 = \frac{4\zeta^2\omega_o^6\omega^2}{((\omega_o^2 - \omega^2)^2 \ + \ 4\zeta^2\omega_o^2\omega^2)^2} \tag{A.18}$$

$$Re(H(j\omega))^2 + Im(H(j\omega))^2 = \frac{\omega_o^4(\omega_o^2 - \omega^2)^2 \ + \ 4\zeta^2\omega_o^6\omega^2}{((\omega_o^2 - \omega^2)^2 \ + \ 4\zeta^2\omega_o^2\omega^2)^2} \tag{A.19}$$

$$Re(H(j\omega))^2 + Im(H(j\omega))^2 = \frac{\omega_o^4((\omega_o^2 - \omega^2)^2 \ + \ 4\zeta^2\omega_o^2\omega^2)}{((\omega_o^2 - \omega^2)^2 \ + \ 4\zeta^2\omega_o^2\omega^2)^2} \tag{A.20}$$

$$|H(j\omega)| = \sqrt{\frac{\omega_o^4}{((\omega_o^2 - \omega^2)^2 \ + \ 4\zeta^2\omega_o^2\omega^2)^2}} = \frac{\omega_o^2}{\sqrt{(\omega_o^2 - \omega^2)^2 \ + \ 4\zeta^2\omega_o^2\omega^2}} \tag{A.21}$$

Set equal to the half-power point:

$$|H(j\omega)| = \frac{\omega_o^2}{\sqrt{(\omega_o^2 - \omega^2)^2 \ + \ 4\zeta^2\omega_o^2\omega^2}} \ = \frac{1}{\sqrt{2}} \tag{A.22}$$

Cross multiply, substitute $\omega = \omega_c$ and solve for ω_c :

$$2\omega_o^4 = (\omega_o^2 - \omega_c^2)^2 \ + \ 4\zeta^2\omega_o^2\omega_c^2 \tag{A.23}$$

$$2\omega_o^4 = \omega_o^4 - 2\omega_o^2\omega_c^2 + \omega_c^4 \ + \ 4\zeta^2\omega_o^2\omega_c^2 \tag{A.24}$$

$$\omega_c^4 + \omega_c^2\left(4\zeta^2\omega_o^2 - 2\omega_o^2\right) - \omega_o^4 = 0 \tag{A.25}$$

Use the quadratic equation to solve for ω_c^2:

$$\omega_c^2 = \frac{-\left(4\zeta^2\omega_o^2 - 2\omega_o^2\right) \pm \sqrt{\left(4\zeta^2\omega_o^2 - 2\omega_o^2\right)^2 - (4)(1)(-\omega_o^4)}}{2(1)} \tag{A.26}$$

$$\omega_c^2 = \frac{\left(2\omega_o^2 - 4\zeta^2\omega_o^2\right) \pm \sqrt{16\zeta^4\omega_o^4 - 16\zeta^2\omega_o^4 + 4\omega_o^4 + 4\omega_o^4}}{2} \tag{A.27}$$

$$\omega_c^2 = \frac{2\left(\omega_o^2 - 2\zeta^2\omega_o^2\right) \pm \sqrt{4\omega_o^4(4\zeta^4 - 4\zeta^2 + 2)}}{2} \tag{A.28}$$

$$\omega_c^2 = \frac{2\omega_o^2\left(1 - 2\zeta^2\right) \pm 2\omega_o^2\sqrt{4\zeta^4 - 4\zeta^2 + 2}}{2} \tag{A.29}$$

$$\omega_c^2 = \omega_o^2(1 - 2\zeta^2 \pm \sqrt{4\zeta^4 - 4\zeta^2 + 2}) \tag{A.30}$$

Taking the square root of ω_c:

$$\omega_c = \omega_o * \sqrt{1 - 2\zeta^2 \pm \sqrt{4\zeta^4 - 4\zeta^2 + 2}} \tag{A.31}$$

Finally, divide by 2π to set from radians to hertz:

$$f_c = \frac{\omega_c}{2\pi} = \left(\omega_o * \sqrt{1 - 2\zeta^2 \pm \sqrt{4\zeta^4 - 4\zeta^2 + 2}}\right) * \frac{1}{2\pi} \tag{A.32}$$

$$f_c = f_n * \sqrt{1 - 2\zeta^2 \pm \sqrt{4\zeta^4 - 4\zeta^2 + 2}} \tag{A.33}$$

Using a subtraction operator in the square root results in a complex number. Thus, the $\pm$ is changes to a $+$ sign and the calculation concludes to:

$$f_c = f_n * \sqrt{1 - 2\zeta^2 + \sqrt{4\zeta^4 - 4\zeta^2 + 2}} \tag{A.34}$$

Equation A.34 demonstrates the corner frequency regardless of changes to the quality factor. To calculate the phase ϕ, take the inverse tangent and divide the imaginary by the real part of the transfer function:

$$\phi = \angle H(\omega) = tan^{-1}\left(\frac{Im\left(H\left(j\omega\right)\right)}{Re\left(H\left(j\omega\right)\right)}\right) \tag{A.35}$$

$$\phi = \angle H(\omega) = tan^{-1}\left(\frac{-2\zeta\omega_o^3\omega}{(\omega_o^2 - \omega^2)^2 \ + \ 4\zeta^2\omega_o^2\omega^2} * \frac{(\omega_o^2 - \omega^2)^2 \ + \ 4\zeta^2\omega_o^2\omega^2}{\omega_o^2(\omega_o^2 - \omega^2)}\right) \tag{A.36}$$

$$\phi = \angle H(\omega) = -tan^{-1}\left(\frac{2\zeta\omega_o\omega}{\omega_o^2 - \omega^2}\right) \tag{A.37}$$

To render the phase in degrees:

$$\phi = \angle H(\omega) = -\frac{180\ ^\circ}{\pi} * tan^{-1}\left(\frac{2\zeta\omega_o\omega}{\omega_o^2 - \omega^2}\right) \tag{A.38}$$

A.4 Significance of Derivation

In a 2^{nd} order lowpass filter, the natural frequency is equal to the corner frequency only when $Q = \zeta = \frac{1}{\sqrt{2}}$. This filter is known as a Butterworth filter of which the corner/natural frequency can be quickly determined by Equation A.4. Any other value for the quality factor and the corner frequency is replaced by Equation A.34. The more that the quality factor deviates from $Q = \frac{1}{\sqrt{2}}$, the further away the corner frequency shifts from the natural frequency.

Appendix B

Analysis of Senior Project Design

B.1 Summary of Functional Requirements

The intention of this project is to build an audio loop station. An audio loop station is an electronic device that is comprised of analog and digital design which allows a musician to record a sample of music in real time. The musician continues to play while the sample loops *ad nauseum*.

B.2 Primary Constraints

Designing for audio projects is cumbersome as audio is easily corrupted by noise and distortion. Component selection is difficult as desired values and package size for resistors and capacitors are not always available. For example, although using film and C0G capacitors is ideal, capacitors are unavailable in 0805 packages for values greater than 0.1 µF. Metal foil resistors offer the best results. However, one metal foil resistor costs $15 to $20, compared to $0.25 to $0.50 which is the price of a thin-film or thick-film resistor.

Size is another challenge to overcome. Though 0805 components make hand-soldering and assembling easier, 0402 or 0201 components will reduce the size of the unit significantly. Mounting the three AA batteries on the PCB took up a great deal of space and could be avoided by using a 9 V_{DC} battery that unattached from the board.

B.3 Economic

A new challenge that will arise if this project is manufactured on a large scale is to mass produce while cutting costs. Typically, audio loop pedals cost from $50 to $400. As shown in Table B.1, producing a prototype of this pedal costs over $135.

A quick comparison on mouser demonstrates that passive components are a fifth of the cost when purchased in bulk versus bought individually and integrated chips – ADC, DAC, microprocessor, op-amp – are roughly half of the original cost when purchased in bulk. Reducing the size of the components and dismounting the power supply from the unit will make the PCB and enclosure less expensive. Two switches can be reduced to one at the expense of complexity to the user.

In order to make this endeavor economically viable, several thousand units should be manufactured every production cycle with a minimum of one production cycle per year is necessary. This is consistent with the market as over one million guitar pedals are sold annually in the United States.

Table B.1: Bill of Materials

Name	Quantity	Description	Ref. Des.	Part Number	Manufacturer	Unit Cost	Total Cost
10µF	5	CAP CER 10UF 10V X7R 0805	C21, C22, C23, C26, C42	08056C106KAT2A	AVX	$0.64	$3.20
4.7µF	7	CAP CER 4.7UF 25V X7R 0805	C15, C16, C17, C18, C34, C35, C36	08053C475MAT2A	AVX	$0.45	$3.15
1µF	2	CAP CER 1UF 16V X7R 0805	C28, C29	08051C105K4Z2A	AVX	$0.47	$0.94
0.1µF	23	CAP CER 0.1UF 16V X7R 0805	C1, C2, C3, C4, C5, C6, C7, C8, C9, C10, C11, C12, C13, C14, C19, C20, C24, C27, C31, C38, C40, C43, C44	ECP-U1C104MA5	Panasonic	$0.57	$13.11
10000pF	1	CAP FILM 10000PF 25V 0805	C25	ECH-U1C103GX5	Panasonic	$0.46	$0.46
5600pF	1	CAP FILM 5600PF 16V 0805	C39	ECH-U1C562JX5	Panasonic	$0.47	$0.47
3300pF	1	CAP FILM 3300PF 25V 0805	C32	ECH-U1C332GX5	Panasonic	$0.37	$0.37
1800pF	1	CAP FILM 1800PF 16V 0805	C41	ECH-U1H182JX5	Panasonic	$0.49	$0.49
1000pF	1	CAP FILM 1000PF 25V 0805	C33	ECH-U1H102JX5	Panasonic	$0.44	$0.44
10pF	1	CAP CER 10PF 50V C0G 0805	C37	08053A100KAT2A	AVX	$0.26	$0.26
Enclosure	1	Enclosure	-	1550D	Hammond	$11.40	$11.40
PCB	1	Printed Circuit Board	-	-	JLCPCB	$11.30	$11.30
Panel Mount LED - YELLOW	1	Panel Mount LED - YELLOW	D1	SSI-LXR1612YD	Lumex	$3.40	$3.40
Panel Mount LED - RED	1	Panel Mount LED - RED	D3	SSI-LXR1612ID	Lumex	$2.94	$2.94
Panel Mount LED - GREEN	1	Panel Mount LED - GREEN	D5	SSI-LXR1612GD	Lumex	$3.19	$3.19
BAT54SWT1G	4	DIODE ARRAY SCHOTTKY 30V SOT323	D2, D4, D6, D7	BAT54SWT1G	ON Semiconductor	$0.21	$0.84
SWD-HDR	1	10 PIN DEBUG HEADER	J1	67997-410HLF	Amphenol FCI	$0.28	$0.28
CONN-JST-B2B-XH-A	6	JST Connector	J2, J4, J6, J8, J9, J11	B2B-XH-A(LF)(SN)	JST	$0.17	$1.02
CONN-JST-B3B-XH-A	3	JST Connector	J3, J5, J10	B3B-XH-A(LF)(SN)	JST	$0.18	$0.54
Battery Holder - 3-AA	1	3 AA series battery holder	J7	2464RB	Keystone Electronics	$1.94	$1.94
Mosfet - N-Ch, logic-level	2	MOSFET SOT-23 N-CH LOGIC	Q1, Q2	BSS138	TI National Semiconductor	$0.26	$0.52
1M	1	RES SMD 1M OHM 1% 1/8W 0805	R20	MCU08050C1004FP500	Vishay	$0.29	$0.29
100k	3	RES SMD 100K OHM 0.5% 1/8W 0805	R14, R16, R24	TNPW0805100KFEEA	Vishay	$0.41	$1.23
56k	12	RES SMD 56K OHM 1% 1/8W 0805	R5, R6, R7, R9, R12, R13, R21, R22, R27, R28	RT0805FRE0756KL	Yageo	$0.12	$1.44
12.1k	1	RES SMD 12.1K OHM 1% 1/8W 0805	R26	TNPW080512K1FEEA	Vishay	$0.11	$0.11
10k	4	RES SMD 10K OHM 1% 1/8W 0805	R2, R3, R4, R10	TNPW080510K0FEEA	Vishay	$0.41	$1.64
1k	2	RES SMD 1K OHM 1% 1/8W 0805	R18, R25	TNPW08051K00FEEA	Vishay	$0.41	$0.82
100	1	RES SMD 100 OHM 1% 1/8W 0805	R17	TNPW0805100RFEEA	Vishay	$0.41	$0.41
54.9	3	RES SMD 54.9 OHM 1% 1/8W 0805	R1, R8, R11	RT0805FRE0754R9L	Yageo	$0.23	$0.69
16-Mbit (1 M × 16) Static RAM	1	16-Mbit (1 M × 16) SRAM	U1	CY62167DV30LL-55ZXI	Cypress	$19.77	$19.77
ICN-R01001-01	1	Renesas S5D5 ARM Cortex M4 120MHz MCU LQFP144	U2	R7FS5D57C3A01CFB#AA0	Renesas	$14.36	$14.36
OPA2376AID	2	Precision, Low Noise, Low Quiescent Current Operational Amplifier, 2 to 5.5 V, -40 to 125 degC, 8-pin SOIC (D8), Green (RoHS & no Sb/Br)	U3, U7	OPA2376AID	Texas Instruments	$2.66	$5.32
LP5907	1	low-noise LDO that can supply up to 250 mA output current	U4	LP5907MFX-3.3/NOPB	Texas Instruments	$0.55	$0.55
LTC1864LCMS8#PBF	1	IC ADC 16-BIT 1CH 150KSPS 8-MSOP	U5	LTC1864LCMS8#PBF	Analog Devices	$14.40	$14.40
DAC8830IBD	1	16-Bit, Ultra-Low Power, Voltage Output Digital to Analog Converter, -40 to 85 degC, 8-pin SOIC (D8), Green (RoHS & no Sb/Br)	U6	DAC8830IBD	Texas Instruments	$14.04	$14.04
					Total	**$135.33**	

B.4 Environmental

Electronic waste is a massive global problem that only continues to grow. Rather than being recycled, refurbished, or properly discarded, most e-waste ends up in landfills where the toxic elements of the electronics pollutes the soil, air, and water. Placing a notice on this product advising users to discard appropriately when the product is at the end of its life cycle prevents irresponsible disposal.

B.5 Manufacturability

Two obstacles to overcome during manufacturing are assembly and programming. This prototype was hand-soldered and programmed with an SWD adapter. This method is not practical for a mass-produced product. A pick-and-place machine will easily place the components on to the PCB to be wave soldered or reflow soldered. With respect to programming, the firmware can be loaded

into the microprocessor by use of a commercial programmer. Conversely, the option of buying microprocessors with pre-loaded firmware is available when purchasing in bulk.

B.6 Sustainability

Once the product is purchased, it will work adequately until the end of its life cycle if the user supplies fresh batteries. Thus, this product is limited by the life cycle of its components. Typically, manufacturers guarantee a guitar pedal for a minimum of one year. However, as users typically purchase pedals as one-time purchases, a good rule of thumb is to have a product last at least five years.

B.7 Ethical

Ethics holds a unique and complex place in the music industry for various reasons. Foreign made instruments, once considered as mediocre products for beginners, are now considered professionally crafted products. Ukuleles, ten-string guitars, electric mandolins, and miniature basses, once considered niche markets, have all successfully crossed over to the mainstream in the age of social media. Quality from Asian markets has increased which, coupled with the rise of YouTube and Facebook creating a platform for niche instruments, has further driven a higher demand on instruments from China, Taiwan, Korea, and Indonesia. The largest audio pedal manufacturers deal exclusively in foreign factories, namely Boss, Behringer, and Danelectro while American made instruments are largely relegated to small-scale shops that produce boutique instruments and amplifiers.

This presents a problem from two standpoints. Unfortunately, instrument manufacturers have one of the worst track records with respect to human rights violations. Millions of instruments across the globe are continuously manufactured in sweatshops in under less-than-ideal environments. Every year representatives from watchdog groups and former sweatshop workers protest at the largest music industry expo, the Anaheim NAMM show, hoping to bring awareness to the conditions for workers in foreign countries. Sadly, the response from instrument manufacturers has been lethargic and unsympathetic. In 2007, guitar manufacturer Cort responded to a worker protest by laying off all employees at one of their manufacturing plants. This prompted workers to stage a hunger strike, several workers to commit suicide out of desperation, and some workers to set themselves on fire as an act of final protest. This maleficence has caused government involvement in various countries to circumvent the use of forced labor, child labor, and at least some semblance of healthy working conditions.

The other catalyst for change is being caused by artist involvement. Many celebrity instrumentalists, such as Tom Morello of Rage Against the Machine and Serj Tankian of System of a Down, have stood in solidarity with foreign workers and withdrawn their support for the companies that they once endorsed. Modern instrument start-ups rely heavily on brand endorsements and having an esteemed artist endorse or condemn your product weighs heavily on public image. In the interest of promoting virtuous business practices and enticing would-be celebrity sponsors it is vital to ensure that high standards be set on work conditions during the manufacturing process.

B.8 Health and Safety

This product presents no risk to the consumer. The primary health concern during manufacturing is to provide a safe place for workers who are properly compensated. A source of danger comes from soldering components to the printed circuit board. Standard procedures for assemblers such as face masks, safety glasses, and a well-ventilated room will minimize health and safety concerns.

B.9 Social and Political

Electronic pedal producers typically outsource manufacturing to Asian markets in an effort to reduce labor and component costs. Though this practice saves money it leaves the manufacturer at risk to several vulnerabilities. Import tariffs are an ever-present reality that may worsen by the increasing tension between the United States and China. Intellectual property theft by foreign actors is easier when production does not take place in-house. Without control of the day-to-day production, it is impossible to assess what product quality might look like. Problems may be difficult to overcome with any language barrier.

B.10 Development

Prior to the development of this project, my experience was relegated to breadboards and protoboards using through-hole components. As audio is a sensitive science, using a PCB with surface mount components was critical, especially since half of this project is digital in nature. Thus, it was mandatory to become familiarized with the characteristics of passive components such as the differences and tradeoffs between Class I, Class II, Electrolytic, and Tantalum capacitors as well as the material characteristics of different types of resistors.